cmgh
CELLULAR AND MOLECULAR GASTROENTEROLOGY AND HEPATOLOGY

ORIGINAL RESEARCH

Activation of Proneuronal Transcription Factor Ascl1 in Maternal Liver Ensures a Healthy Pregnancy

Joonyong Lee,[1] Veronica Garcia,[1] Shashank M. Nambiar,[1] Huaizhou Jiang,[1,2] and Guoli Dai[1]

[1]Department of Biology, School of Science, Indiana University–Purdue University Indianapolis, Indianapolis, Indiana; and
[2]School of Traditional Chinese Medicine, Anhui University of Chinese Medicine, Hefei, China

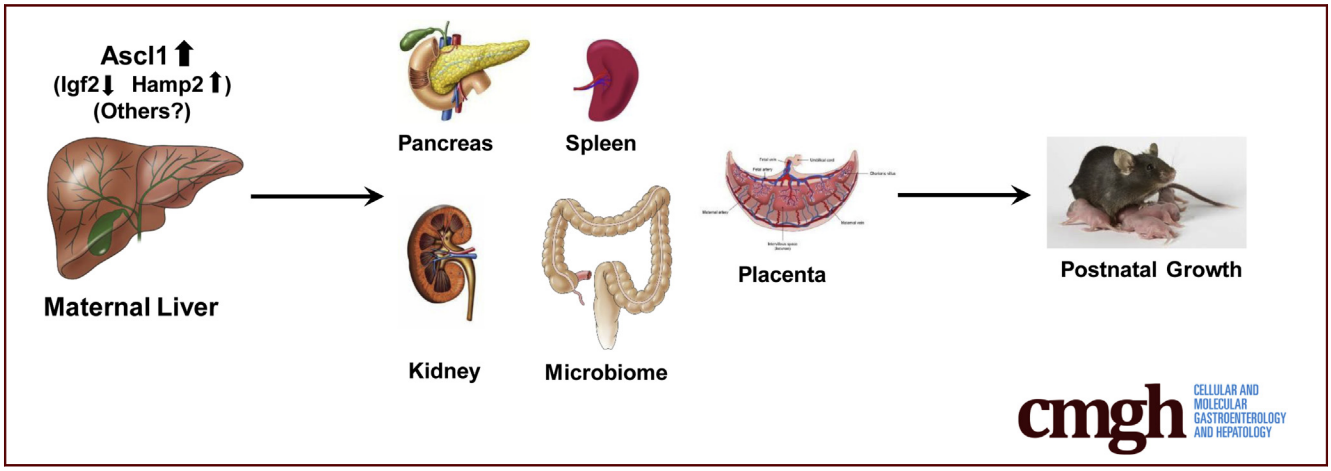

SUMMARY

How the maternal liver adapts to pregnancy remains elusive. We found that maternal liver activates the expression of *Ascl1*, a gene encoding a proneuronal transcription factor, to coordinate the adaptations of maternal organs and the growth of the placenta, enabling a healthy pregnancy and normal postnatal growth of the offspring.

BACKGROUND & AIMS: Maternal liver shows robust adaptations to pregnancy to accommodate the metabolic needs of the developing and growing placenta and fetus by largely unknown mechanisms. We found that *Ascl1*, a gene encoding a basic helix-loop-helix transcription factor essential for neuronal development, is highly activated in maternal hepatocytes during the second half of gestation in mice.

METHODS: To investigate whether and how *Ascl1* plays a pregnancy-dependent role, we deleted the *Ascl1* gene specifically in maternal hepatocytes from midgestation until term.

RESULTS: As a result, we identified multiple *Ascl1*-dependent phenotypes. Maternal livers lacking *Ascl1* showed aberrant hepatocyte structure, increased hepatocyte proliferation, enlarged hepatocyte size, reduced albumin production, and increased release of liver enzymes, indicating maternal liver dysfunction. Simultaneously, maternal pancreas and spleen and the placenta showed marked overgrowth; and the maternal ceca microbiome showed alterations in relative abundance of several bacterial subpopulations. Moreover, litters born from maternal hepatic *Ascl1*-deficient dams experienced abnormal postnatal growth after weaning, implying an adverse pregnancy outcome. Mechanistically, we found that maternal hepatocytes deficient for *Ascl1* showed robust activation of insulin-like growth factor 2 expression, which may contribute to the *Ascl1*-dependent phenotypes widespread in maternal and uteroplacental compartments.

CONCLUSIONS: In summary, we show that maternal liver, via activating *Ascl1* expression, modulates the adaptations of maternal organs and the growth of the placenta to maintain a healthy pregnancy. Our studies show that *Ascl1* is a novel and critical regulator of the physiology of pregnancy. *(Cell Mol Gastroenterol Hepatol 2022;13:35–55; https://doi.org/10.1016/j.jcmgh.2021.08.009)*

Keywords: Hepatocyte; Gestation; Insulin-Like Growth Factor 2.

Abbreviations used in this paper: 4E-BP1, eukaryotic translation initiation factor 4E-binding protein 1; AAV8, adeno-associated virus 8; AKT, protein kinase B; Ascl1, achaete-scute homolog-like 1; cDNA, complementary DNA; ERK, extracellular signal-regulated kinase; GD, gestation day; IGF2, insulin-like growth factor 2; IGF2R, IGF2 receptor; ISH, in situ hybridization; mRNA, messenger RNA; P, promoter; PL, placental lactogen; qRT-PCR, quantitative reverse-transcription polymerase chain reaction; RNA-seq, RNA sequencing; TBG-Cre, Cre recombinase under the control of hepatocyte-specific thyroxine-binding globulin promoter.

Most current article

2352-345X
https://doi.org/10.1016/j.jcmgh.2021.08.009

The establishment and maintenance of pregnancy requires highly coordinated adaptations in maternal, uteroplacental, and fetal compartments. As pregnancy progresses, in the maternal compartment, the liver grows to expand its metabolic capacity[1]; the pancreas proliferates its β-cell population to increase insulin production[2]; the gut alters its microbiome, contributing to immunologic adjustments[3]; the spleen undergoes development and growth of the erythroid lineage[4,5]; and the kidney expands its volume, allowing for increases in blood flow and fluid retention.[6–8] These adaptations of maternal nonreproductive organs to pregnancy must be required to meet the demands of the developing and growing placenta and fetus. However, the physiological significance and the regulatory mechanisms of these processes are poorly understood, representing an emerging research field.

We and others have shown that the maternal liver undergoes hyperplasia and hypertrophy, changes its gene expression profile, and thereby markedly expands during gestation in rodents.[1,9,10] However, how this is controlled remains elusive. We previously showed that the expression of achaete-scute homolog-like 1 (*Ascl1*), a gene encoding a basic helix-loop-helix transcription factor essential for neurogenesis,[11–13] is highly up-regulated in maternal livers of pregnant rats.[14] During development, *Ascl1* controls proliferation, cell-cycle exit, and full neuronal differentiation and specification of neural progenitor cells in both the central and peripheral nervous systems.[12,15,16] *Ascl1* inhibits its own expression by negative autoregulation in the developing nervous system, possibly explaining the lack of overt abnormalities in *Ascl1*$^{+/-}$ mice,[17] whereas *Ascl1*$^{-/-}$ pups die within hours after birth as a result of defects in brain development.[11] In the adult, *Ascl1* is expressed only in the brain and spinal cord, where there is ongoing neurogenesis, and in developing neuroendocrine cells in multiple organs including the cerebellum, thyroid, and thymus.[18] In this study, we evaluated the activation, and explored the function, of *Ascl1* in maternal livers of pregnant mice. We found that *Ascl1* not only modulates maternal hepatic adaptation, but also mediates the communication of maternal liver with other maternal organs and the placenta, eventually affecting pregnancy outcomes.

Results

Ascl1 *Is Highly Activated in Maternal Hepatocytes*

We first evaluated the expression of *Ascl1* in maternal livers throughout the course of gestation in mice. As pregnancy advanced, its transcript levels in maternal livers were increased progressively, reaching up to 26,000-fold on gestation days 13 and 15, relative to the prepregnancy state (Figure 1*A*). Maternal hepatic *Ascl1* protein was expressed abundantly as its messenger RNA (mRNA) levels peaked on these 2 gestation days (Figure 1*B*). *Ascl1* transcript was detected exclusively in maternal hepatocytes (Figure 1*C*). In human beings, *Ascl1* mRNA was expressed abundantly in a maternal liver of a pregnant woman, and in livers with diseases such as hepatocellular carcinoma, hepatocellular adenoma, and hepatitis (Figure 1*D*). *Ascl1* transcript was not detectable by in situ hybridization (ISH) in maternal pancreas, spleen, kidney, and the placenta in gestation day 15 mice (Figure 2*A*). *Ascl1* mRNA expression was marginally detected by quantitative reverse-transcription polymerase chain reaction (qRT-PCR), but did not show significant gestation-dependent changes in maternal kidney on gestation days 8 (early pregnancy), 13 (midgestation), and 18 (late pregnancy) (Figure 2*B*). *Ascl1* transcript levels were below detection by qRT-PCR in maternal pancreas and spleen on those gestation days. The data indicate that the activation of *Ascl1* expression is not a generalized phenomenon in the maternal compartment. Thus, it is truly astonishing that pregnancy activates a proneuronal transcription factor in an epithelial cell type (maternal hepatocytes) in such a striking magnitude in both animals and human beings, strongly suggesting a gestation-dependent role for this transcription factor.

Adeno-Associated Virus 8 Containing the Gene for Cre Recombinase Under the Control of Hepatocyte-Specific Thyroxine-Binding Globulin Promoter Efficiently Deletes Ascl1 *in Maternal Hepatocytes*

Ascl1 is activated in maternal liver during the second half of pregnancy, suggesting a role in the maintenance of pregnancy. To determine this, we took a loss-of-function approach to delete the *Ascl1* gene specifically in maternal hepatocytes from midgestation to term and evaluated how pregnancy was affected. We generated timed pregnancies in *Ascl1*$^{fl/fl}$ female mice by mating them with *Ascl1*$^{+/+}$ males. This led to a homogeneous *Ascl1*$^{+/fl}$ fetal genotype. Adeno-associated virus 8 (AAV8)–Cre recombinase under the control of hepatocyte-specific thyroxine-binding globulin promoter (TBG-Cre) virus or AAV8 virus with a null vector (control) virus was injected into *Ascl1*$^{fl/fl}$ mice on gestation day 8. Mice were killed on gestation days 15 and 18 for phenotypic assessment. This AAV8-TBG virus has been shown to specifically infect hepatocytes with more than 99% efficiency in mice.[19–21] qRT-PCR analysis showed that *Ascl1* mRNA was almost completely lost in maternal livers of pregnant animals treated with the AAV8–TBG-Cre virus (Figure 3*A*), indicating highly efficient *Ascl1* gene deletion in this organ. As such, mice deficient for *Ascl1* in maternal hepatocytes are referred to as hep-*Ascl1*$^{-/-}$ mice hereafter. We observed massive AAV8–TBG-Cre virus-mediated recombination in maternal hepatocytes in gestation day 18 hep-*Ascl1*$^{-/-}$ mice. We detected the recombination in the islets of maternal pancreas, in few cells in maternal kidneys, but not in maternal spleen and the placenta (Figure 3*B*). In a pretest study, we detected green fluorescent protein (GFP) expression in maternal livers but not in fetal livers after injecting AAV8-TBG-GFP reporter virus into pregnant mice. This indicates that the AAV8 virus does not effectively pass through the placenta to infect the fetuses.

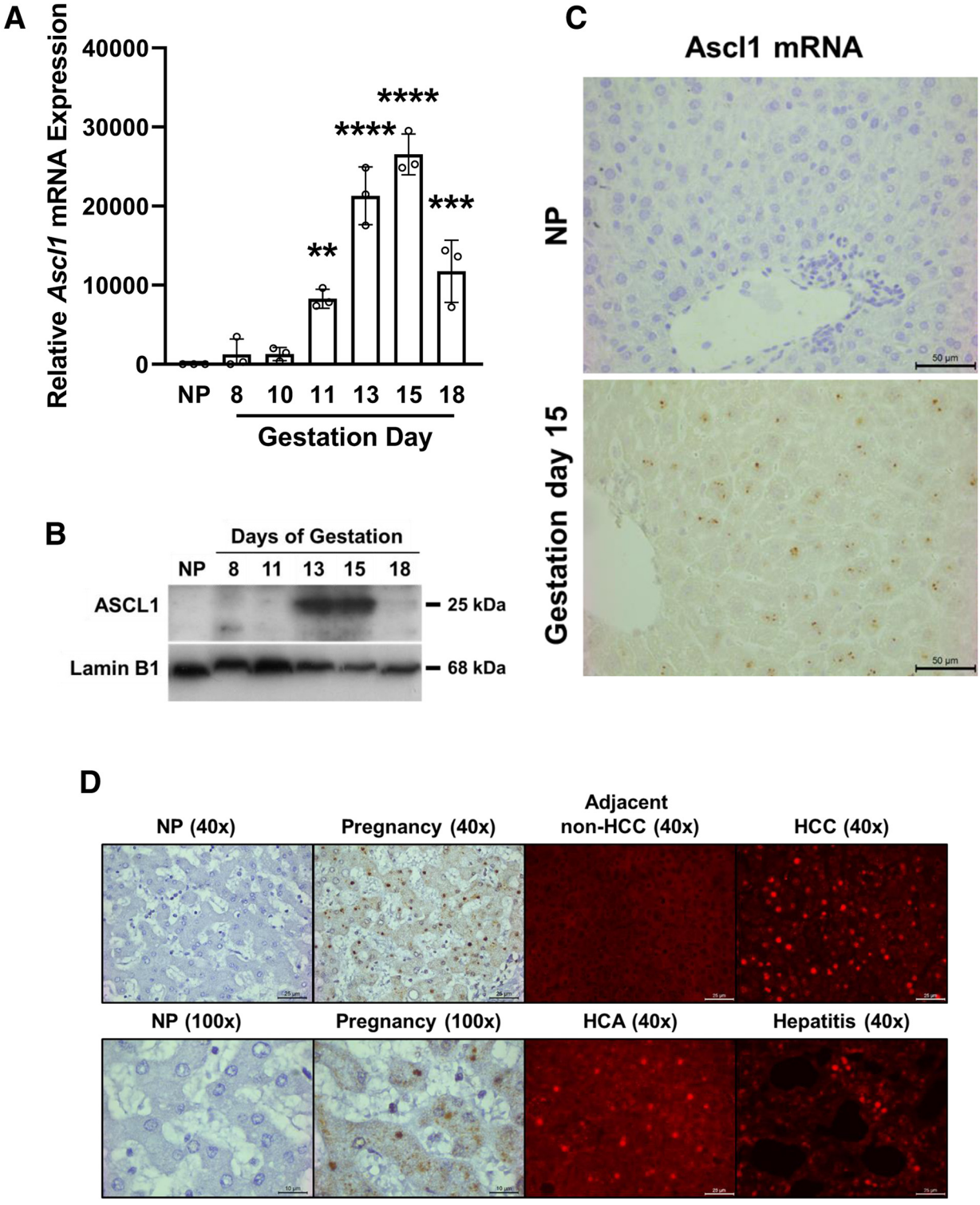

Figure 1. *Ascl1* activation in maternal livers of pregnant mice and human beings. Timed pregnancies were generated in 3-month-old C57BL/6 female mice. Livers were collected from nonpregnant (NP) mice and maternal livers from pregnant mice at the indicated GDs. (*A–C*) *Ascl1* expression in maternal livers. (*A*) Hepatic *Ascl1* mRNA levels were measured using qRT-PCR and presented as the mean fold changes relative to NP controls ± SD (n = 3). $^{**}P < .01$, $^{***}P < .001$, and $^{****}P < .0001$, compared with NP controls. (*B*) Western blot was performed using liver nuclear lysates with antibodies against ASCL1. Lamin B1 was used as a loading control. (*C*) Liver sections were subjected to *Ascl1* in situ hybridization. *Ascl1* mRNA is stained dark brown. (*D*) Liver sections were prepared from archived paraffin blocks of human liver tissues. *Ascl1* mRNA was visualized on liver sections. Representative results are shown with liver sections from a NP woman, a 6 months' pregnant mother, a hepatocellular carcinoma (HCC) patient, a hepatocellular adenoma (HCA) patient, and a 4.5-month-old child with hepatitis.

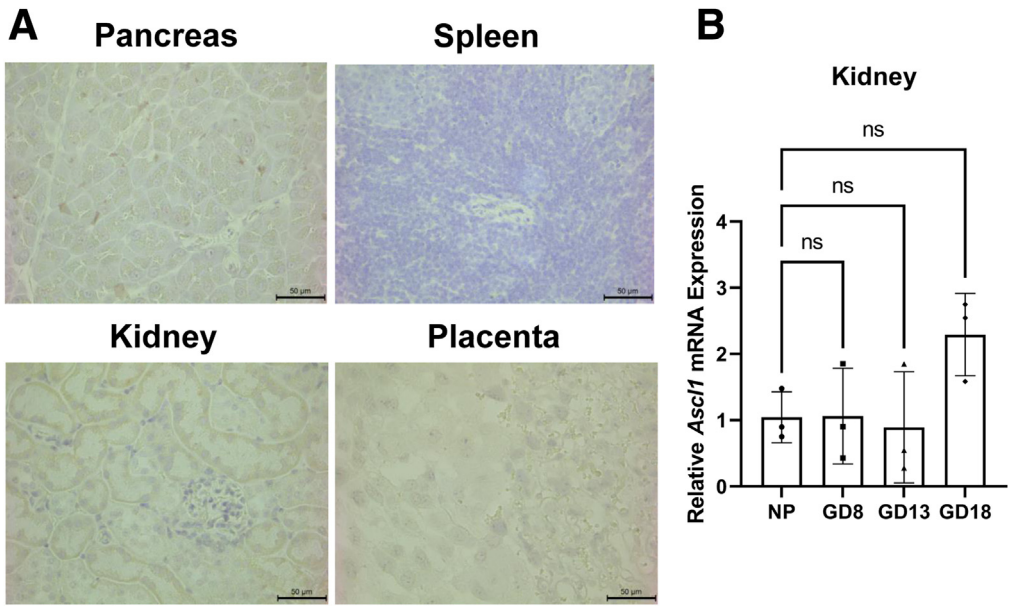

Figure 2. *Ascl1* mRNA expression in maternal nonhepatic organs of pregnant mice. Timed pregnancies were generated in 3-month-old C57BL/6 female mice. Maternal organs were collected from nonpregnant (NP) mice and pregnant mice at the indicated GDs. (*A*) The sections of maternal organs and the placenta isolated from GD15 mice were subjected to *Ascl1* in situ hybridization. (*B*) *Ascl1* mRNA levels in maternal kidneys were measured using qRT-PCR and are presented as the mean fold changes relative to NP controls ± SD (n = 3).

RNA-Sequencing Analysis Shows Ascl1*-Dependent Transcriptome in Maternal Liver*

We next compared the transcriptomes of gestation day 15 maternal livers between the 2 genotype groups of mice by RNA sequencing (RNA-seq) to profile potential *Ascl1* target genes in this context. This showed 1274 differentially expressed genes. They were either up-regulated or down-regulated by at least 2-fold with a false-discovery rate of less than 0.05 when maternal hepatic *Ascl1* was lacking (Figure 3*C*). Pathway analysis suggests that these genes are associated with many biological processes including the metabolism of hormones (eg, melatonin), neurotransmitters (eg, serotonin and dopamine), fatty acids, alcohol, carbohydrates, nucleic acids, and amino acids, cell-cycle control, cell function and maintenance, and vitamin D–receptor/retinoid X–receptor activation (Figure 3*D*). These data imply that *Ascl1* directly or indirectly regulates a broad spectrum of genes and thereby possesses multiple functions in maternal liver in this physiological state (pregnancy).

Hepatocyte-Specific Ascl1 *Knockout Results in Maternal Liver Abnormalities*

We subsequently assessed whether maternal livers showed *Ascl1*-dependent phenotypes. Compared with maternal hepatocytes sufficient for *Ascl1*, maternal hepatocytes lacking *Ascl1* showed an aberrant structure (eosin staining–negative around the nuclei) (Figure 4*A*), enhanced hepatocyte proliferation (Figure 4*B* and *F*), and increased size (Figure 4*C* and *G*), hence causing further enlargement of the maternal liver (Figure 4*D* and *E*). These abnormalities were accompanied by reduced albumin mRNA expression and protein production and increased circulating alanine aminotransferase (Figure 4*H*). These observations indicate that *Ascl1* loss of function in maternal hepatocytes impairs their structure and function.

Hepatocyte-Specific Ascl1 *Knockout Causes Overgrowth of Maternal Pancreas, Spleen, and Kidney*

We additionally examined several other maternal organs to estimate whether there were *Ascl1*-dependent systemic effects in the maternal compartment. Surprisingly, without maternal hepatic *Ascl1*, the maternal pancreas nearly doubled in size (Figure 5*A* and *B*), had a reduced proportion of insulin-positive areas (Figure 5*C* and *D*), and unchanged total β-cell mass (Figure 5*E*), while the concentrations of circulating insulin and nonfasting blood glucose were unaltered (Figure 5*F* and *G*). These data suggest that *Ascl1* inactivation in maternal liver stimulates the expansion of the exocrine component without interfering with the pregnancy-dependent growth of the endocrine component in the maternal pancreas. Similarly, the maternal spleen also almost doubled in volume with overtly expanded red and white pulps (Figure 6*A*–*C*), while the maternal kidney showed enlargement without an obvious histologic alteration (Figure 6*D* and *E*). Collectively, we conclude that the loss of function of *Ascl1* in maternal hepatocytes imposes systematic effects, causing overgrowth of at least a subset of maternal organs.

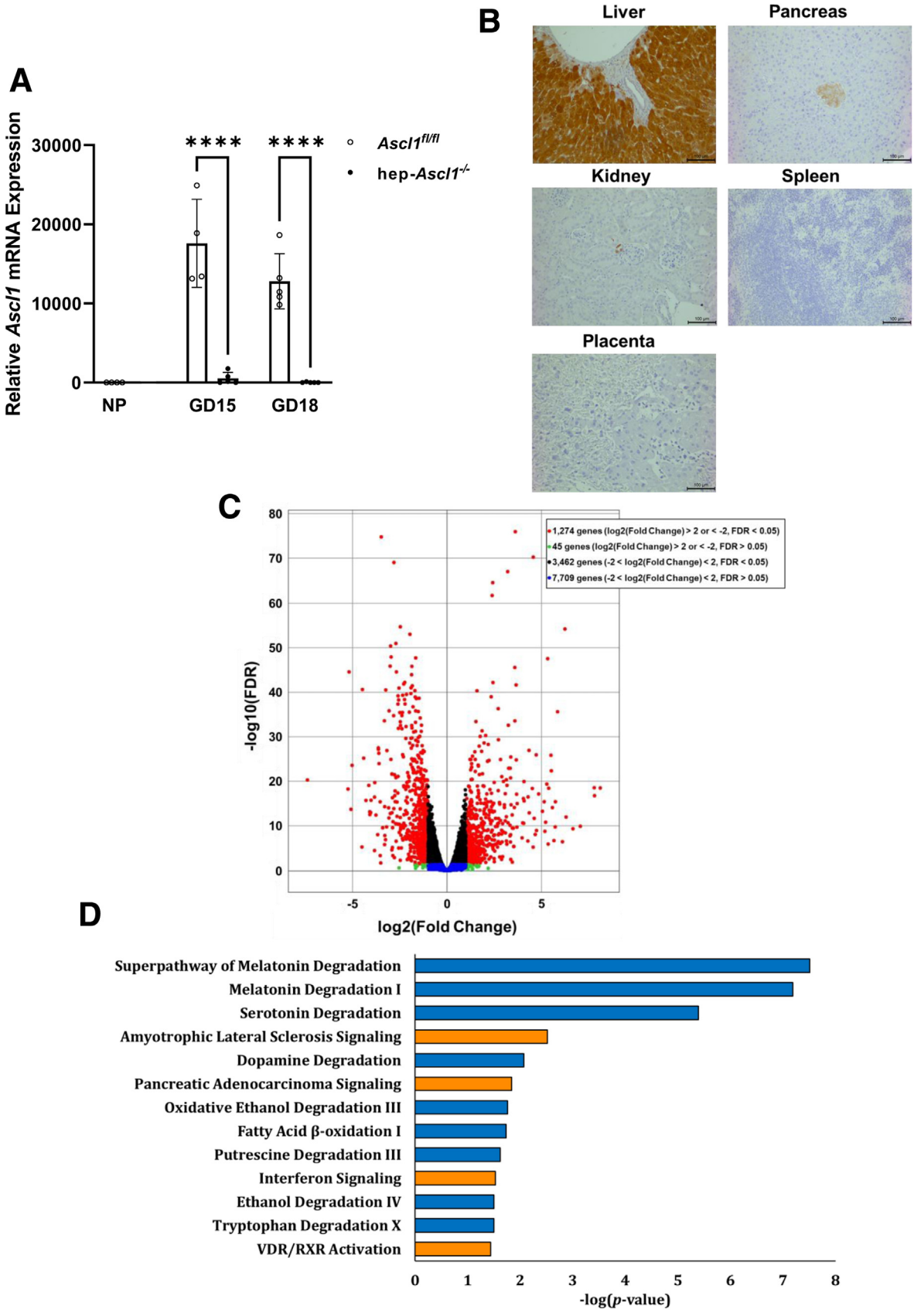
A
Relative Ascl1 mRNA Expression
30000
20000
10000
0
****
****
Ascl1fl/fl
hep-Ascl1-/-
NP
GD15
GD18
B
Liver
Pancreas
Kidney
Spleen
Placenta
C
1,274 genes (log2(Fold Change) > 2 or < -2, FDR < 0.05)
45 genes (log2(Fold Change) > 2 or < -2, FDR > 0.05)
3,462 genes (-2 < log2(Fold Change) < 2, FDR < 0.05)
7,709 genes (-2 < log2(Fold Change) < 2, FDR > 0.05)
-log10(FDR)
log2(Fold Change)
D
Superpathway of Melatonin Degradation
Melatonin Degradation I
Serotonin Degradation
Amyotrophic Lateral Sclerosis Signaling
Dopamine Degradation
Pancreatic Adenocarcinoma Signaling
Oxidative Ethanol Degradation III
Fatty Acid β-oxidation I
Putrescine Degradation III
Interferon Signaling
Ethanol Degradation IV
Tryptophan Degradation X
VDR/RXR Activation
-log(p-value)

Hepatocyte-Specific Ascl1 *Knockout Leads to Abnormal Maternal Cecal Microbiota*

It is known that the maternal gut microbiome undergoes pregnancy-dependent changes, which are associated with the health of both the mother and the fetus.[22] To determine whether maternal hepatic *Ascl1* is relevant to the maternal microbiome, we collected maternal cecal contents from gestation day 18 hep-*Ascl1*$^{-/-}$ mice and *Ascl1*$^{fl/fl}$ (control) mice, and compared their microbiome profiles via 16S sequencing (Figure 7*A*). Most notably, *Ascl1* loss in maternal hepatocytes resulted in the following: (1) a complete depletion of *Pseudobutyrivibrio–Roseburia intestinalis*, which protects colonic mucosa against inflammation,[23] (2) the appearance of *Desulfovibrio oxamicus–vulgaris*, which metabolizes a variety of chemicals,[24] and (3) alterations in the relative abundance of 6 other bacteria species. Furthermore, RNA-seq analysis showed that *Hamp2*, a gene encoding hepcidin antimicrobial peptide 2, which has a strong antimicrobial activity against certain bacteria,[25,26] depends on *Ascl1* for expression. This finding was confirmed by qRT-PCR (Figure 7*B*). Together, we show that maternal hepatic *Ascl1* modulates the adaptation of the maternal microbiota to pregnancy, potentially via regulating *Hamp2*.

Hepatocyte-Specific Ascl1 *Knockout Causes Placental Overgrowth and Aberrant Postnatal Growth of Offspring*

We examined the uteroplacental and fetal compartments and postnatal growth of pups to determine whether *Ascl1* deficiency in maternal hepatocytes ultimately affects pregnancy outcomes. Compared with the placentas of control mice, the placentas of hep-*Ascl1*$^{-/-}$ mice were enlarged markedly, manifested by a 26.9% increase in weight on gestation day 15 and a 33% increase on gestation day 18, with the expansion of both the junctional and labyrinth zones (Figure 8*A* and *B*). The distribution of glycogen trophoblast cells visualized by glycogen staining did not appear to be *Ascl1*-dependent (Figure 8*C*). By in situ hybridization, we probed the mRNAs of placental lactogen (*PL*)-*I*, a marker gene for parietal trophoblast giant cells,[27] and *PL-II*, a marker gene for parietal trophoblast giant cells, spongiotrophoblast cells, and labyrinth trophoblast giant cells,[27] and did not observe an overt *Ascl1*-dependent distribution of these trophoblast cell populations (Figure 8*D*). These results of placental structural evaluations suggest that the loss of function of *Ascl1* in maternal hepatocytes causes placental overgrowth without disrupting placental structure. Moreover, when comparing hep-*Ascl1*$^{-/-}$ pregnant mice with their control mice, the placental levels of insulin-like growth factor (IGF2), a potent placental and fetal growth factor,[28–30] were reduced by 32% on gestation day 15, but were equivalent on gestation day 18, whereas placental concentration of *PL*-II, a major hormone produced by the placenta during the second half of gestation,[31] was unchanged (Figures 8*E* and 9). However, when maternal hepatic *Ascl1* was deficient, maternal blood concentration of alkaline phosphatase, an enzyme elaborated primarily from the placenta and a marker for trophoblast differentiation,[32] was increased significantly on gestation day 15 and more than 2-fold on gestation day 18 (Figure 8*F*). The data of these functional assessments suggest that *Ascl1* inactivation in maternal hepatocytes partially influences placental function.

Furthermore, it is known that protein kinase B (AKT) and extracellular signal-regulated kinase (ERK) signaling critically regulates placental development and growth.[33,34] We found that, without *Ascl1* in maternal hepatocytes, placental AKT1 phosphorylation at S473, but not at T308, was increased mildly; in contrast, ERK1 and ERK2 activities were inhibited dramatically, reduced by as much as 80% and 76%, respectively, before parturition (gestation day 18) (Figures 8*E* and 9). Thus, the loss of maternal hepatic *Ascl1* results in strong inhibition of placental ERK signaling.

In addition, we did not observe a difference in fetal weight and number on both gestation days 15 and 18 between the 2 genotype groups of mice (Figure 10*A* and *B*). However, compared with those male and female pups born from control dams, male pups born from hep-*Ascl1*$^{-/-}$ dams showed a 16% increase in weekly body weight gain at week 1 after weaning, but a 41% decrease at week 2, while female pups born from hep-*Ascl1*$^{-/-}$ dams showed a 32% increase at week 1, a 35% decrease at week 2, a 38% decrease at week 3, and a 43% increase at week 5 (Figure 10*C* and *D*). Apparently, pups born from the 2 genotype groups of dams grew quite differently after weaning. Taken together, we show that the maternal hepatic *Ascl1* null mutation causes placental overgrowth, partial changes in placental function, severe suppression of placental ERK activity, and an abnormal postnatal growth pattern of offspring.

Figure 3. (***See previous page***). **Differentially expressed genes and canonical pathways affected by hepatocyte-specific deletion of *Ascl1* in the maternal liver.** AAV8-TBG-Cre virus or AAV8 virus with a null vector (AAV8-TBG-null) control virus was injected via tail vein at a dose of 1×10^{12} genomic copies per mouse on GD8 *Ascl1*$^{fl/fl}$ mice. (*A*) Total RNA was isolated from livers of nonpregnant (NP) and GD15 and GD18 *Ascl1*$^{fl/fl}$ and hepatocyte-specific *Ascl1* knockout (hep-*Ascl1*$^{-/-}$) mice. Hepatic *Ascl1* mRNA levels were measured using qRT-PCR and presented as the mean fold changes relative to NP controls ± SD (n = 4–5). ****$P < .0001$. (*B*) AAV8-TBG-Cre virus–mediated recombination in maternal organs and the placenta. The sections of maternal organs and the placenta collected from GD18 hep-*Ascl1*$^{-/-}$ mice were subjected to immunostaining with a GFP antibody. (*C* and *D*) *Ascl1*-dependent transcriptome. Total RNA was isolated from livers of *Ascl1*$^{fl/fl}$ and hep-*Ascl1*$^{-/-}$ mice on GD15 and was subjected to RNA-seq (n = 4–5). (*C*) Differentially expressed genes are presented by the volcano plot. Red: significantly up-regulated or down-regulated genes; black, green, and blue: nonsignificant genes. Differentially expressed genes with at least 2-fold and $P < .05$ were analyzed using the Ingenuity Pathway Analysis. (*D*) The top enriched canonical pathways targeted by hepatic Ascl1 are presented. Orange, up-regulated; blue, down-regulated. FDR, false-discovery rate; GFP, green fluorescent protein; VDR/RXR, vitamin D receptor/retinoid X receptor.

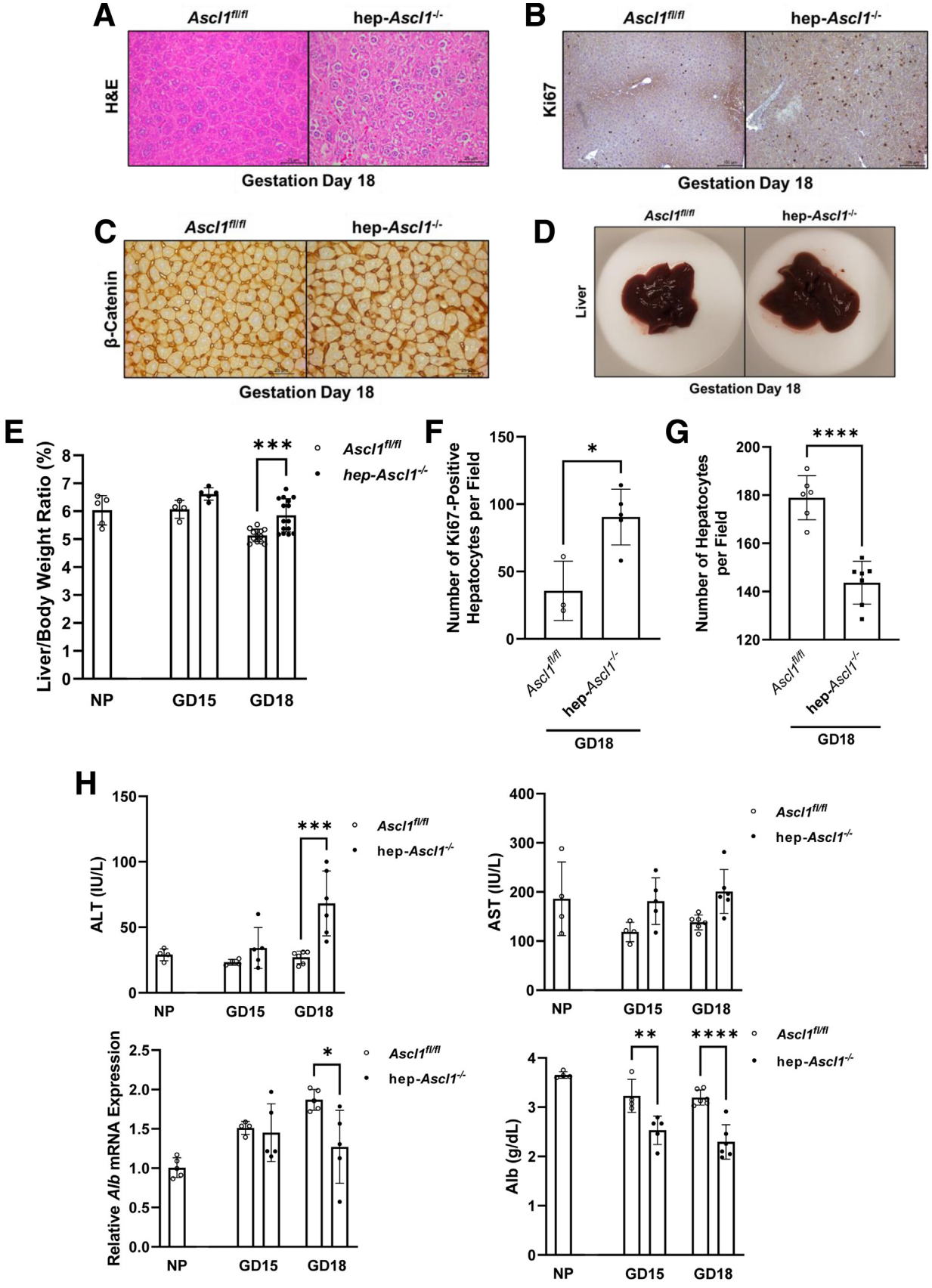
A
Ascl1fl/fl
hep-Ascl1-/-
H&E
Gestation Day 18
B
Ascl1fl/fl
hep-Ascl1-/-
Ki67
Gestation Day 18
C
Ascl1fl/fl
hep-Ascl1-/-
β-Catenin
Gestation Day 18
D
Ascl1fl/fl
hep-Ascl1-/-
Liver
Gestation Day 18
E
Liver/Body Weight Ratio (%)
***
Ascl1fl/fl
hep-Ascl1-/-
NP
GD15
GD18
F
Number of Ki67-Positive Hepatocytes per Field
*
Ascl1fl/fl
hep-Ascl1-/-
GD18
G
Number of Hepatocytes per Field
****
Ascl1fl/fl
hep-Ascl1-/-
GD18
H
ALT (IU/L)
***
Ascl1fl/fl
hep-Ascl1-/-
NP
GD15
GD18
AST (IU/L)
Ascl1fl/fl
hep-Ascl1-/-
NP
GD15
GD18
Relative Alb mRNA Expression
*
Ascl1fl/fl
hep-Ascl1-/-
NP
GD15
GD18
Alb (g/dL)
**
****
Ascl1fl/fl
hep-Ascl1-/-
NP
GD15
GD18

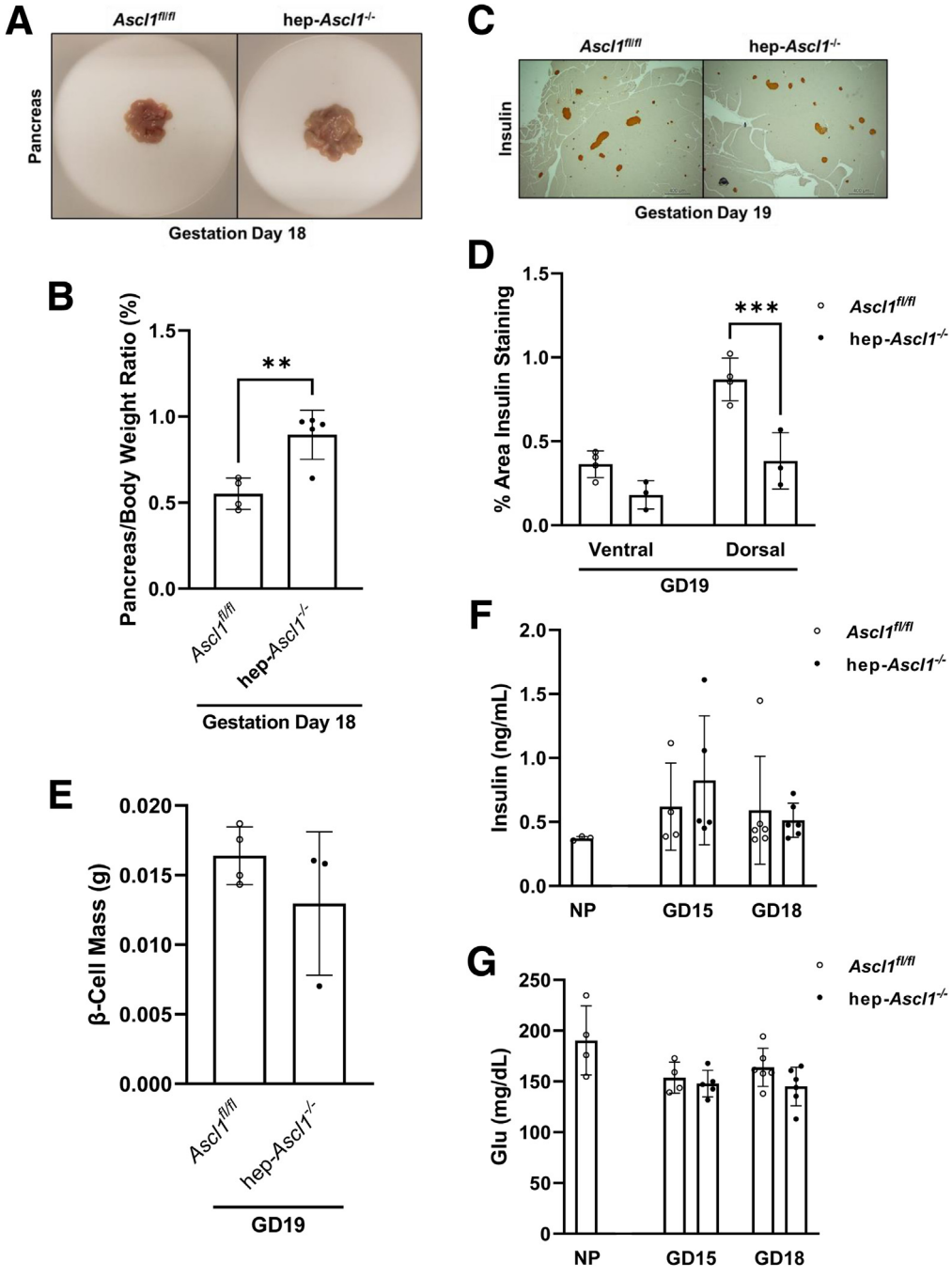

Figure 5. Maternal pancreas phenotypes in maternal hepatocyte-specific *Ascl1* ablated mice. Maternal pancreases were collected and weighed from nonpregnant (NP) and GD18 or GD19 *Ascl1*$^{fl/fl}$ and hep-*Ascl1*$^{-/-}$ mice. (*A*) Morphology of the pancreas. (*B*) Maternal pancreas-to-total-body-weight ratios are presented as means ± SD (n = 4–5). (*C*) Maternal pancreatic sections were subjected to insulin immunostaining. (*D*) The quantification of the insulin-positive islets to the pancreatic section area are presented as means ± SD (n = 3–4). (*E*) β-cell mass is presented as the means ± SD (n = 3–4). Serums were collected from NP and GD15 and GD18 *Ascl1*$^{fl/fl}$ and hep-*Ascl1*$^{-/-}$ mice. Serum (*F*) insulin and (*G*) glucose are presented as the means ± SD (n = 3–6). $^{**}P < .01$, and $^{***}P < .001$. Glu, glucose.

Figure 4. (***See previous page***). **Maternal liver phenotypes in maternal hepatocyte-specific *Ascl1* ablated mice.** Livers were collected and weighed from nonpregnant (NP) and GD15 and GD18 *Ascl1*$^{fl/fl}$ and hep-*Ascl1*$^{-/-}$ mice. (*A*) Liver sections were stained with H&E. Liver sections were subjected to (*B*) Ki67 and (*C*) β-catenin staining. (*D*) Morphology of *Ascl1*$^{fl/fl}$ and hep-*Ascl1*$^{-/-}$ mouse livers. (*E*) Liver-to-body-weight ratios are presented as means ± SD (n = 4–10). (*F*) Ki67- and (*G*) β-catenin–positive hepatocytes were counted in 5 random fields of view (magnification, ×200) per section and presented as the means ± SD (n = 3–7 per group). (*H*) Serums were collected from NP and pregnant *Ascl1*$^{fl/fl}$ and hep-*Ascl1*$^{-/-}$ mice. Data from the serum biochemical profile are expressed as means ± SD (n = 5). Hepatic albumin mRNA levels were measured using qRT-PCR and presented as the mean fold changes relative to NP controls ± SD (n = 4–5). $^{*}P < .05$, $^{**}P < .01$, $^{***}P < .001$, and $^{****}P < .0001$. Alb, albumin; ALT, alanine aminotransferase; AST aspartate aminotransferase.

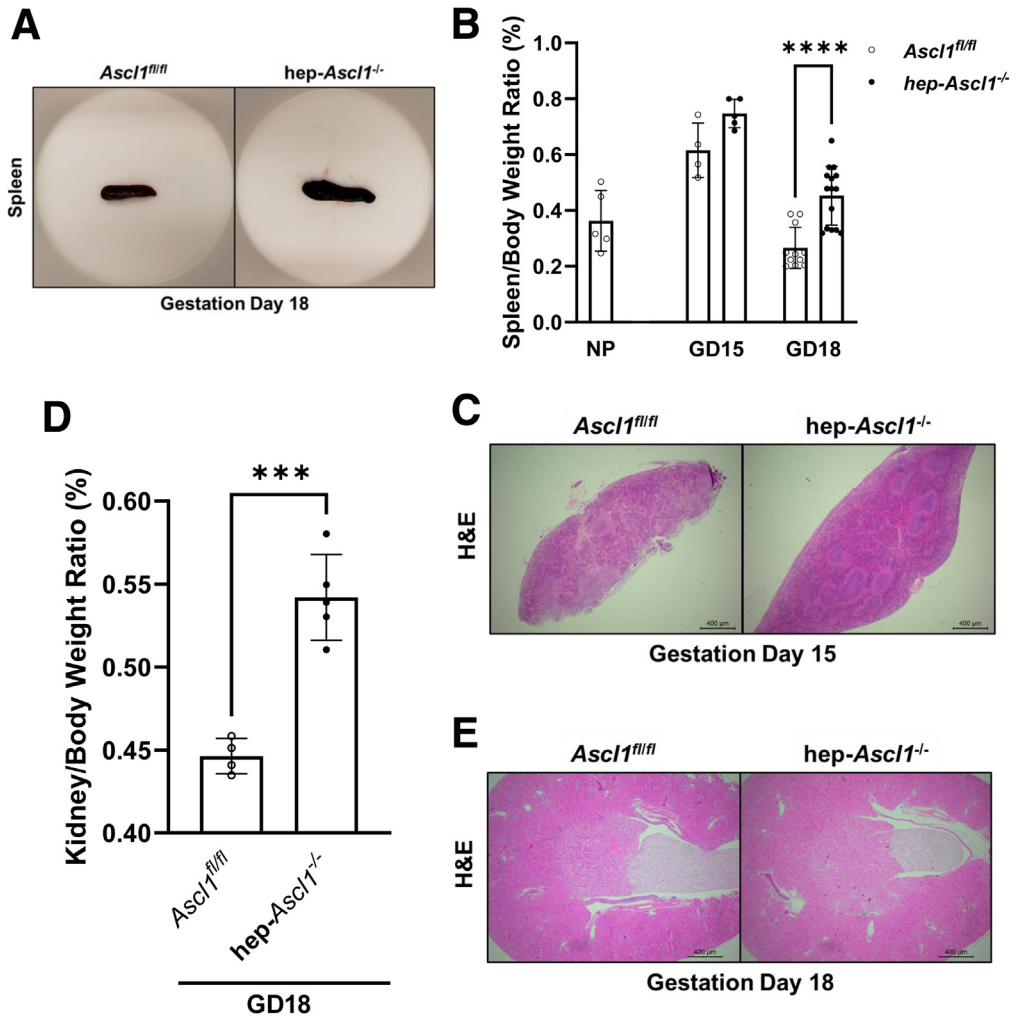

Figure 6. Maternal spleen and kidney phenotypes in maternal hepatocyte-specific *Ascl1* ablated mice. Maternal spleens and kidneys were collected and weighed from nonpregnant (NP) and GD15 and GD18 *Ascl1*$^{fl/fl}$ and hep-*Ascl1*$^{-/-}$ mice. (*A*) Morphology of the spleens. (*B*) Spleen-to-total-body-weight ratios are presented as means ± SD (n = 4–10). (*C*) Splenic sections were stained with H&E. (*D*) Kidney-to-total-body-weight ratios are presented as means ± SD (n = 4–5). (*E*) Kidney sections were stained with H&E. ***$P < .01$ and ****$P < .0001$.

Hepatocyte-Specific Ascl1 *Knockout Leads to* Igf2 *Activation in Maternal Hepatocytes*

The earlier-described observations that several maternal organs were enlarged significantly in hep-*Ascl1*$^{-/-}$ pregnant mice relative to controls prompted us to look for growth factors regulated by *Ascl1* from our RNA-seq analysis. We found 1 candidate: *Igf2*, which encodes a potent growth factor[28–30] and was induced with *Ascl1* loss. To validate the RNA-seq data, we quantified *Igf2* mRNA levels by qRT-PCR in maternal livers of gestation days 15 and 18 and show that the loss of *Ascl1* in maternal hepatocytes induced robust *Igf2* mRNA expression in maternal livers, most strikingly on gestation day 18 (Figure 11*A*). Consistently, maternal hepatic IGF2 protein was produced abundantly in hep-*Ascl1*$^{-/-}$ pregnant mice, but was undetectable in control pregnant mice (Figure 11*B*). In situ hybridization and immunohistochemistry detected rich *Igf2* transcripts and IGF2 protein in maternal hepatocytes deficient for *Ascl1*, but not in controls (Figure 11*C* and *D*). In mice, *Igf2* is imprinted maternally and is regulated differentially in the placenta and fetus. It is transcribed from 4 promoters, designated *Igf2-P0*, *P1*, *P2*, and *P3*. *Igf2-P0* directs *Igf2* transcription in the placenta, whereas *Igf2-P1*, *P2*, and *P3* direct its transcription in both the placenta and fetus.[29,35] We used a set of qRT-PCR primers to analyze promoter-specific *Igf2* transcripts in maternal livers[36] (Figure 11*E*). We found that *P0* remained silent no matter the presence or absence of *Ascl1* in maternal hepatocytes. In contrast, the other 3 promoters all were activated as a result of *Ascl1* loss in these cells. The concentration of circulating IGF2 protein in gestation day 18 hep-*Ascl1*$^{-/-}$ mice was approximately 9 times higher than that in control mice (Figure 11*F*). These data collectively show that, in maternal hepatocytes, *Ascl1* deficiency results in *Igf2* activation via *P1*, *P2*, and *P3*, creating a maternal environment rich in this growth factor. Thus, here we linked *Igf2* to *Ascl1*-dependent phenotypes in our experimental settings.

To further evaluate IGF2 signaling, we examined the expression and activities of several associated signaling molecules in maternal livers of both genotype groups of mice (Figures 11*B* and 12). We found that, compared with the prepregnancy state, the lack of *Ascl1* in maternal hepatocytes prevented gestation-dependent increases in IGF2

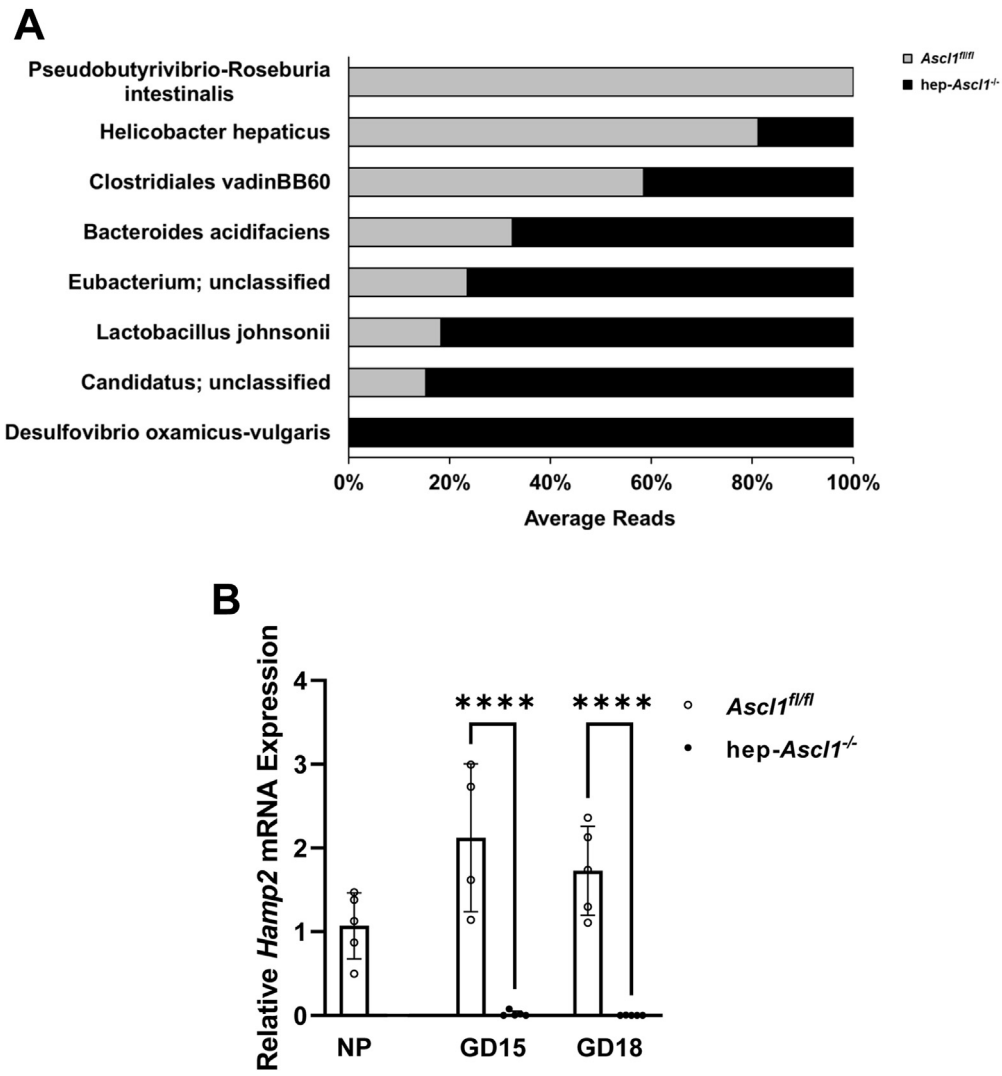

Figure 7. Phenotypes of maternal cecal microbiota in maternal hepatocyte-specific *Ascl1* ablated mice. Maternal cecal samples were collected from GD18 *Ascl1*$^{fl/fl}$ and hep-*Ascl1*$^{-/-}$ mice. (*A*) Cecal microbiota analysis (n = 5). (*B*) Hepatic *Hamp2* mRNA levels were measured using qRT-PCR and presented as the mean fold changes relative to nonpregnant (NP) controls ± SD (n = 4–5). ****$P < .0001$.

receptor (IGF2R) expression; did not affect the activities of phospho-AKT and phospho-ERK; and increased the expression levels of both total and phosphorylated eukaryotic translation initiation factor 4E-binding protein 1 (4E-BP1). The data indicate that *Ascl1* controls IGF2 signaling also via regulating IGF2R, and 4E-BP1 may transduce IGF2 signaling in this setting.

Discussion

It has been an enigma why maternal liver activates a proneuronal gene (*Ascl1*) in response to pregnancy. Here, we show that *Ascl1* is required for the maternal liver to structurally and functionally adapt to this physiological stimulus (pregnancy). Loss of *Ascl1* in maternal hepatocytes impairs their cellular structure, reflected by the formation of a layer of eosin staining–negative substance around their nuclei. This substance was Oil Red O staining–negative and periodic acid–Schiff staining–negative, suggesting that it is not a fatty acid or glycogen. Others reported a similar phenomenon in *Mst1/2* double-knockout hepatocytes.[37] The connection between *Ascl1* and Mst1/2 signaling in maternal hepatocytes will be interesting to explore in the future. Although the eosin staining–negative substance around the hepatocyte nuclei remains unknown, we believe that it is linked to *Ascl1* deficiency–caused dysfunction of maternal hepatocytes, characterized by reduced albumin production and increased alanine aminotransferase and aspartate aminotransferase release. Moreover, *Ascl1* loss induced increased proliferation and hypertrophy of maternal hepatocytes, which was associated with increased IGF2 production by these cells. IGF2 is a prototypical growth factor driving cell expansion and organogenesis during development,[38] and adult regenerating livers activate IGF2 to promote hepatocyte replication.[39] In addition, we found that *Ascl1* also governs IGF2R expression. IGF2R internalizes and degrades IGF2, eliminating excessive IGF2 in tissues and the

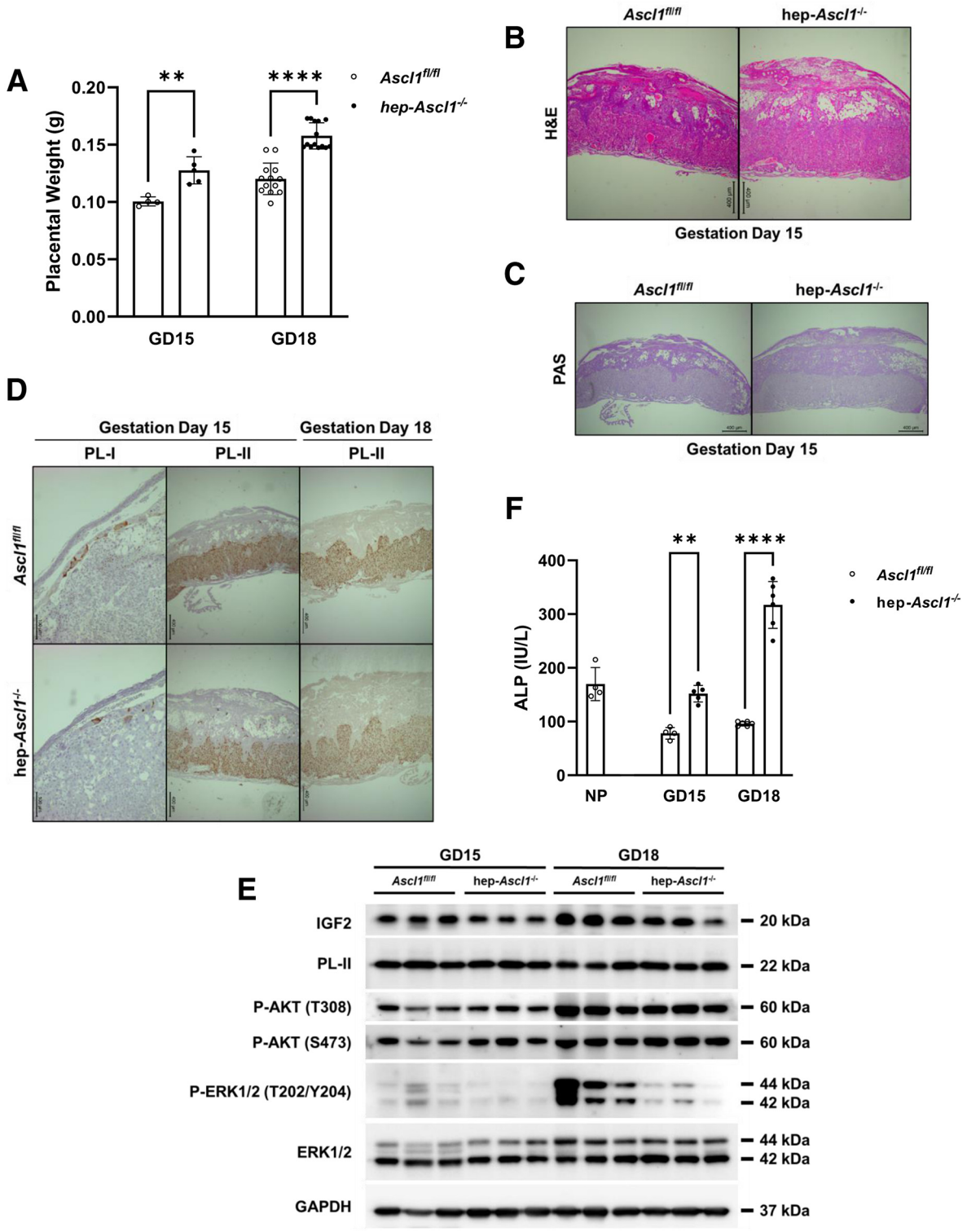

Figure 8. Placental phenotypes in maternal hepatocyte-specific *Ascl1* ablated mice. Placentas were collected and weighed from GD15 and GD18 *Ascl1*$^{fl/fl}$ and hep-*Ascl1*$^{-/-}$ mice. (*A*) Placental weights are presented as means ± SD (n = 4–9 dams). (*B*) Placental sections were stained with H&E. (*C*) Frozen placental sections underwent periodic acid–Schiff (PAS) staining. Glycogen is stained red to purple. (*D*) Frozen placental sections were subjected to *PL*-I and *PL*-II in situ hybridization staining using the RNAscope 2.5 HD Assay-BROWN kit. The *PL*-I and *PL*-II mRNAs are stained dark brown. (*E*) Western blot was performed using placental lysates prepared from 1 placenta per dam with antibodies against the proteins indicated. Glyceraldehyde 3-phosphate dehydrogenase (GAPDH) was used as a loading control. Serums were collected from nonpregnant (NP) and GD15 and GD18 *Ascl1*$^{fl/fl}$ and hep-*Ascl1*$^{-/-}$ mice. (*F*) The concentrations of circulating alkaline phosphatase (ALP) are presented as means ± SD (n = 4–6). $^{**}P < .01$ and $^{****}P < .0001$.

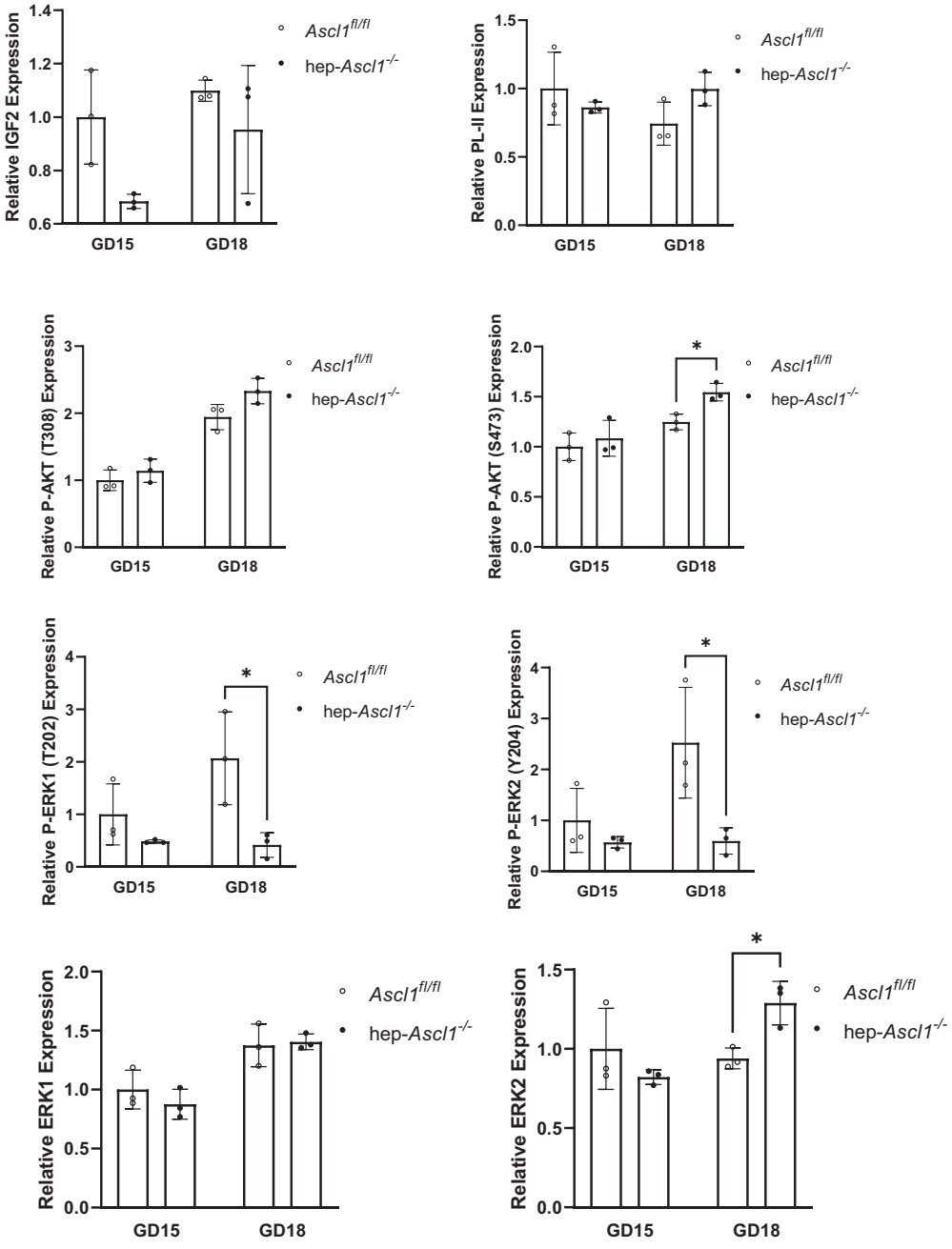

Figure 9. Quantification of relative intensity of Western blot signals from Figure 8*E*. Signal intensity was normalized with glyceraldehyde 3-phosphate dehydrogenase. Data are presented as the mean fold changes relative to GD15 *Ascl1*$^{fl/fl}$ mice ± SD (n = 3). *P < .05.

circulation.[40] Thus, *Ascl1* activation not only ensures the silence of *Igf2*, but also up-regulates IGF2R expression, strictly controlling IGF2 signaling in the maternal compartment. Furthermore, 4E-BP1 is well known for its function of stimulating protein synthesis and cell growth.[41] *Ascl1* deficiency–caused increase in hepatocyte cell size can be explained by increased 4E-BP1 activity in these cells.

Here, we show that pregnancy reprograms maternal hepatocytes to activate *Ascl1*, thereby controlling the transcriptional output and modulating the expression of at least 1274 genes. Of special note, the top canonical pathway describing these differentially expressed genes is one that represents genes involved in the metabolism of neurotransmitters. *Ascl1* is known to be essential for the development of serotonergic and dopaminergic neurons and also regulates their neurotransmitter biosynthesis.[42,43] Remarkably, *Ascl1* alone is sufficient to generate functional neurons from fibroblasts and embryonic stem cells, being a key driver of induced neuronal cell reprogramming in different cell contexts.[44] These findings raise the question of whether *Ascl1* activation enables maternal hepatocytes to possess some properties of neurons as an adaptive response to

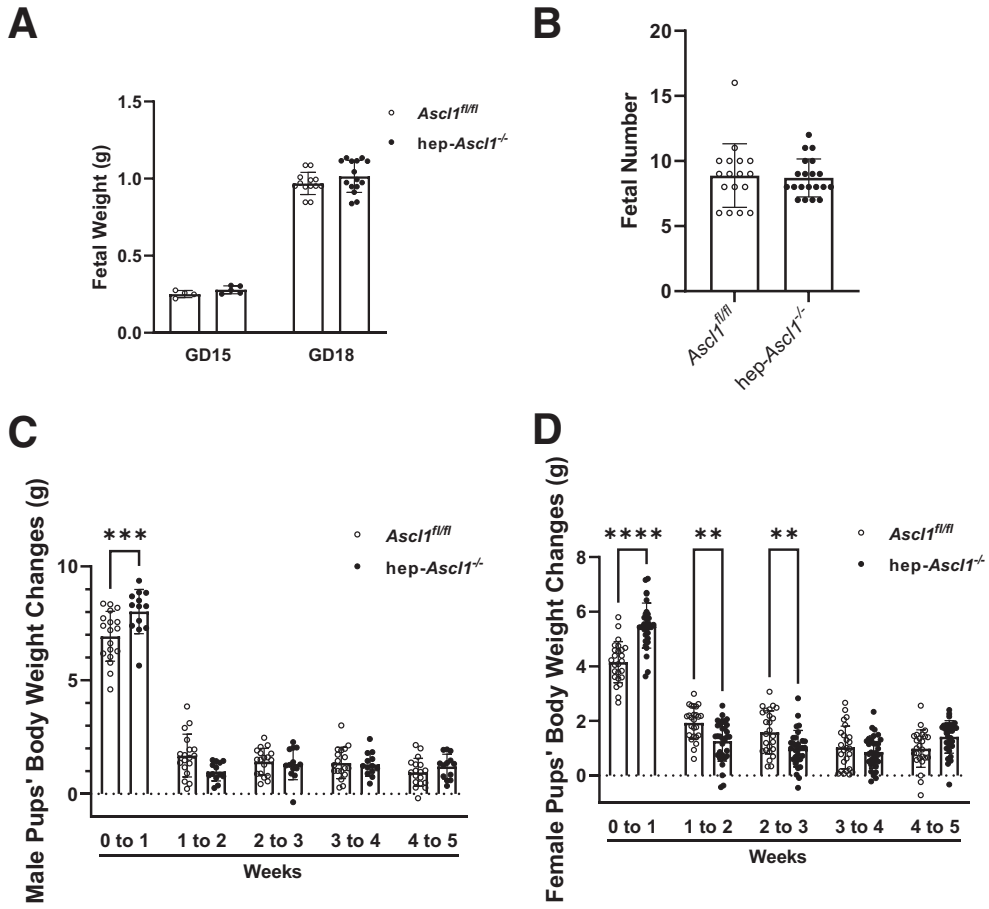

Figure 10. Pregnancy outcomes in maternal hepatocyte-specific *Ascl1* ablated mice. Fetuses were collected and weighed from GD15 and GD18 *Ascl1*$^{fl/fl}$ and hep-*Ascl1*$^{-/-}$ mice. (*A*) Fetal weight and (*B*) numbers are presented as means ± SD (n = 13–31). Weekly body weight changes of weaned (*C*) male and (*D*) female pups are presented as means ± SEM (n = 43 from 5 *Ascl1*$^{fl/fl}$ dams; n = 44 from 6 hep-*Ascl1*$^{-/-}$ dams; n = 6–10 per litter). $^{**}P < .01$, $^{***}P < .001$, and $^{****}P < .0001$.

support a healthy pregnancy. We are very interested in answering this question in our future studies.

It is surprising that inactivating *Ascl1* in maternal liver induced robust systemic responses in the maternal compartment. This implies that the maternal liver, via activating *Ascl1*, communicates with other maternal organs to systematically coordinate maternal adaptations to pregnancy, uncovering a novel function of maternal liver during pregnancy. Moreover, we showed an *Ascl1/Igf2* axis in maternal hepatocytes, where *Ascl1* normally silences the *Igf2* locus and thereby avoids the exposure of other maternal organs to this growth factor. Others reported that *Ascl1* knockdown resulted in an increase in *Igf2* expression in neuronal cells in vitro.[45] Thus, this axis may be operating in both maternal hepatocytes and neurons. We gained further insight into this axis in that IGF2 was derived from 3 placental- and fetal-specific promoters of *Igf2* in maternal hepatocytes without *Ascl1*. How *Ascl1* controls the activities of these 3 promoters of *Igf2* is another question for the future. We believe that this *Ascl1/Igf2* axis, at least in part, underlies *Ascl1*-dependent phenotypes in the maternal compartment. When maternal hepatocyte *Ascl1* is lost, excess IGF2 is produced in, and elaborated from, these cells. Locally, this promotes maternal hepatocyte proliferation and growth. Systemically, it induces overgrowth of maternal pancreas, spleen, and kidney. Through these autocrine and endocrine pathways, IGF2 partially mediates *Ascl1*-dependent phenotypes. It is highly likely that other maternal organs not examined in this study also respond to the null mutation of maternal hepatic *Ascl1*. However, we are unable to exclude the possibility that *Ascl1* expression also is activated in a maternal organ not examined and AAV8-TBG-Cre virus induces recombination there, contributing to *Ascl1*-dependent phenotypes in pregnant mice.

Our studies show that *Ascl1* activation in maternal hepatocytes is required to maintain pregnancy-dependent homeostasis of maternal gut microbiota. It is known that the microbiome shows adaptive changes to accommodate the physiological and immunologic alterations of the host during pregnancy.[22,46,47] Here, we found that 8 bacteria species in maternal ceca responded to the deficiency of maternal hepatic *Ascl1*. Remarkably, among these bacteria species, *Pseudobutyrivibrio–R intestinalis* was depleted and *D oxamicus–vulgaris* appeared aberrantly. The former is known to be associated with the anti-inflammatory activity of colonic mucosa,[23] whereas the latter participates in metabolism of various substances such as ammonium, lactate, alcohol, and pyruvate.[24] Therefore, maternal liver,

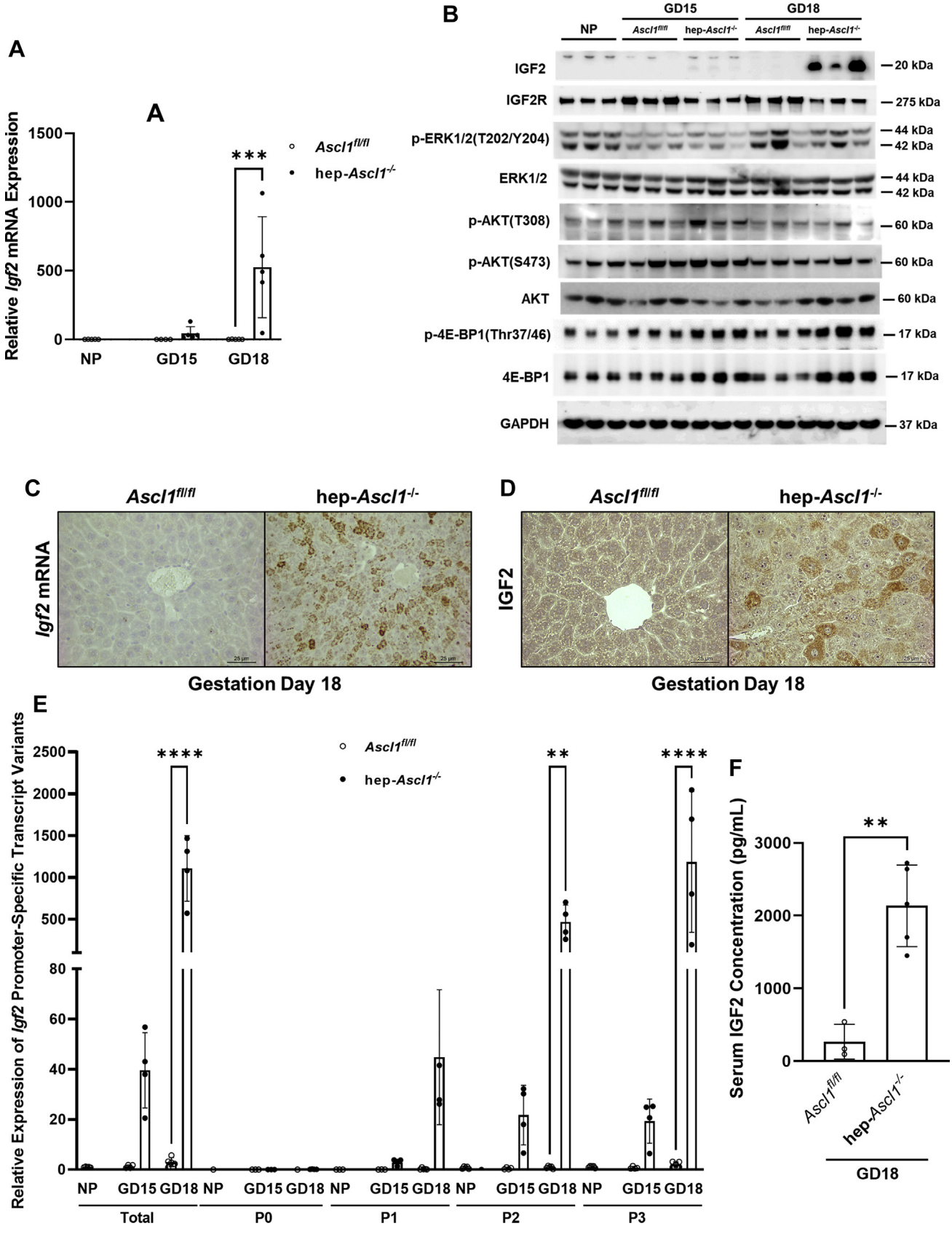
A
A
Relative Igf2 mRNA Expression
1500
1000
500
0
***
Ascl1fl/fl
hep-Ascl1-/-
NP
GD15
GD18
B
GD15
GD18
NP
Ascl1fl/fl
hep-Ascl1-/-
Ascl1fl/fl
hep-Ascl1-/-
IGF2
20 kDa
IGF2R
275 kDa
p-ERK1/2(T202/Y204)
44 kDa
42 kDa
ERK1/2
44 kDa
42 kDa
p-AKT(T308)
60 kDa
p-AKT(S473)
60 kDa
AKT
60 kDa
p-4E-BP1(Thr37/46)
17 kDa
4E-BP1
17 kDa
GAPDH
37 kDa
C
Ascl1fl/fl
hep-Ascl1-/-
Igf2 mRNA
Gestation Day 18
D
Ascl1fl/fl
hep-Ascl1-/-
IGF2
Gestation Day 18
E
Relative Expression of Igf2 Promoter-Specific Transcript Variants
2500
2000
1500
1000
500
80
60
40
20
0
****
**
****
Ascl1fl/fl
hep-Ascl1-/-
NP
GD15
GD18
Total
P0
P1
P2
P3
F
Serum IGF2 Concentration (pg/mL)
3000
2000
1000
0
**
Ascl1fl/fl
hep-Ascl1-/-
GD18

by activating *Ascl1*, controls these 2 bacteria populations in maternal ceca, showing new roles for *Ascl1* in maternal liver. Several lines of evidence suggest that the other 6 bacteria species also are important to the health of the host,[23,24,48–51] however, the gestation-dependent functions of these bacteria species remain unclear. Mechanistically, we identified an *Ascl1/Hamp2* axis in maternal hepatocytes as a candidate regulator of maternal gut microbiota. Our data show that *Hamp2* mRNA expression almost fully relies on *Ascl1* activation in maternal hepatocytes. *Hamp2* is produced primarily in the liver, has strong antimicrobial activity against certain bacteria, and regulates immune responses against bacterial pathogens.[52,53] Hence, we assume that this *Ascl1/Hamp2* axis in maternal hepatocytes may partially govern the adaptations of maternal gut microbiota to gestation.

Our studies show that maternal liver, through activating *Ascl1*, modulates the placenta. This notion is based on our observations that maternal liver *Ascl1* deficiency leads to placenta overgrowth and a change in its function. These phenotypes can be partially interpreted as the consequences of the exposure of the placenta to increased maternal IGF2. We also observed that hep-*Ascl1*$^{-/-}$ placenta transiently reduced its IGF2 production on gestation day 15 and largely diminished its Erk1/2 signaling on gestation day 18 relative to their controls. Thus, the placenta used different mechanisms at distinct stages of pregnancy to defensively respond to increased maternal IGF2, eventually restricting its otherwise further overgrowth. We think that maternal liver activates *Ascl1* to maintain *Igf2* silencing and, by doing this, allows the placenta to appropriately develop and grow without potential maternal inference. It was surprising that the fetal weight was not affected by increased maternal IGF2. This may suggest that the defense responses of the placenta (reduction in IGF2 production and suppression in Erk1/2 activity) to increased maternal IGF2 is so strong that the potential stimulatory effect of this potent hormone on fetal growth is fully blocked. However, we did observe severely impaired postnatal growth of the offspring born from hep-*Ascl1*$^{-/-}$ dams. It is a well-established concept that maternal problems generate long-term adverse effects on the health of the next generation.[54–56] Hence, we believe that *Ascl1* deficiency–caused dysregulation of maternal adaptations and placental abnormality together impair the postnatal growth of the offspring. This model warrants further investigations.

In summary, we show that, as pregnancy advances, maternal hepatocytes activate the expression of *Ascl1* to alter their transcriptomes. Via this mechanism, maternal liver systematically coordinates adaptations in the maternal compartment and allows for optimal placental development and growth, collectively ensuring the health of both the mother and her infant during pregnancy and postnatally.

Methods

Mice

Ascl1$^{fl/fl}$;*R26*$^{EYFP/EYFP}$ mice were a generous gift from Dr Francois Guillemot (The Francis Crick Institute, London, United Kingdom).[57] The mice are referred to hereafter as *Ascl1*$^{fl/fl}$ for simplicity. C57BL/6 mice were purchased from the Jackson Laboratory (Bar Harbor, ME). Mice were maintained on a 12-hour light/12-hour dark cycle (7 AM on and 7 PM off) at 22°C ± 1°C and given standard rodent chow and water ad libitum. Animals were randomly allotted to experimental groups by body weight. All of the animal experiments were conducted in accordance with the National Institutes of Health's *Guide for the Care and Use of Laboratory Animals*. The protocols for the care and use of animals were approved by the Indiana University–Purdue University Indianapolis Animal Care and Use Committee.

Mouse Genotyping

Genomic DNA was prepared from mouse ear snips using the modified hot sodium hydroxide and Tris (HotSHOT) method.[58] All mice were genotyped by PCR using KAPA Taq PCR Kits (Kapa Biosystems, Inc, Wilmington, MA). Specific primers purchased from Integrated DNA Technologies (Coralville, IA) were used to detect the wild-type and mutant alleles. Primers *Ascl1* forward (5'CTACTGTCCAAACGCAAAGTGG3') and *Ascl1* wild-type reverse (5'GCTCCCACAATCCTCGTAAAGA3') were used to detect the *Ascl1* wild-type allele (342 bp), and primers *Ascl1* forward and *Ascl1* mutant reverse (5'TAGACGTTGTGGCTGTTGTAGT3') were used to detect floxed the *Ascl1* allele (857 bp).[59] PCR conditions were as follows: 35 cycles at 94°C for 30 seconds, 69°C for 30 seconds, and 72°C for 90 seconds.

Timed Pregnancy and Virus Injection

Timed pregnancy was generated by mating 3-month-old virgin *Ascl1*$^{fl/fl}$ female mice with wild-type male mice to ensure heterozygous fetuses with 1 wild-type *Ascl1* allele. The presence of a copulation plug in the vagina was designated as gestation day (GD) 1. AAV8-TBG-Cre (AV-8-PV1091; Addgene, Watertown, MA) was injected via tail vein at a dose of 1×10^{12} genomic copies per mouse on GD8, and mice were killed on GD15 and GD18. AAV8 virus with a null vector (AV-8-PV0148; Addgene) was used as a control.

Figure 11. (***See previous page***). ***Igf2* activation in maternal livers deficient for *Ascl1*.** Maternal livers were collected and weighed from nonpregnant (NP) and GD15 and GD18 *Ascl1*$^{fl/fl}$ and hep-*Ascl1*$^{-/-}$ mice. (*A*) Hepatic *Igf2* mRNA levels were measured using qRT-PCR and presented as the mean fold changes relative to NP controls ± SD (n = 4–5). (*B*) Western blot was performed using liver lysates with antibodies against the proteins indicated. (*C*) *Igf2* in situ hybridization on liver sections. (*D*) IGF2 immunostaining. (*E*) Levels of hepatic *Igf2* promoter-specific transcript variants were measured using qRT-PCR and presented as the mean fold changes relative to NP controls ± SD (n = 4–5). (*F*) Levels of IGF2 protein in serum were measured using enzyme-linked immunosorbent assay and presented as the mean fold changes ± SD (n = 3–5). $^{**}P < .01$, $^{***}P < .001$, and $^{****}P < .0001$. P0, placental-specific *Igf2* promoter; P1-3, placental- and fetal liver-specific *Igf2* promoter. GAPDH, glyceraldehyde-3-phosphate dehydrogenase.

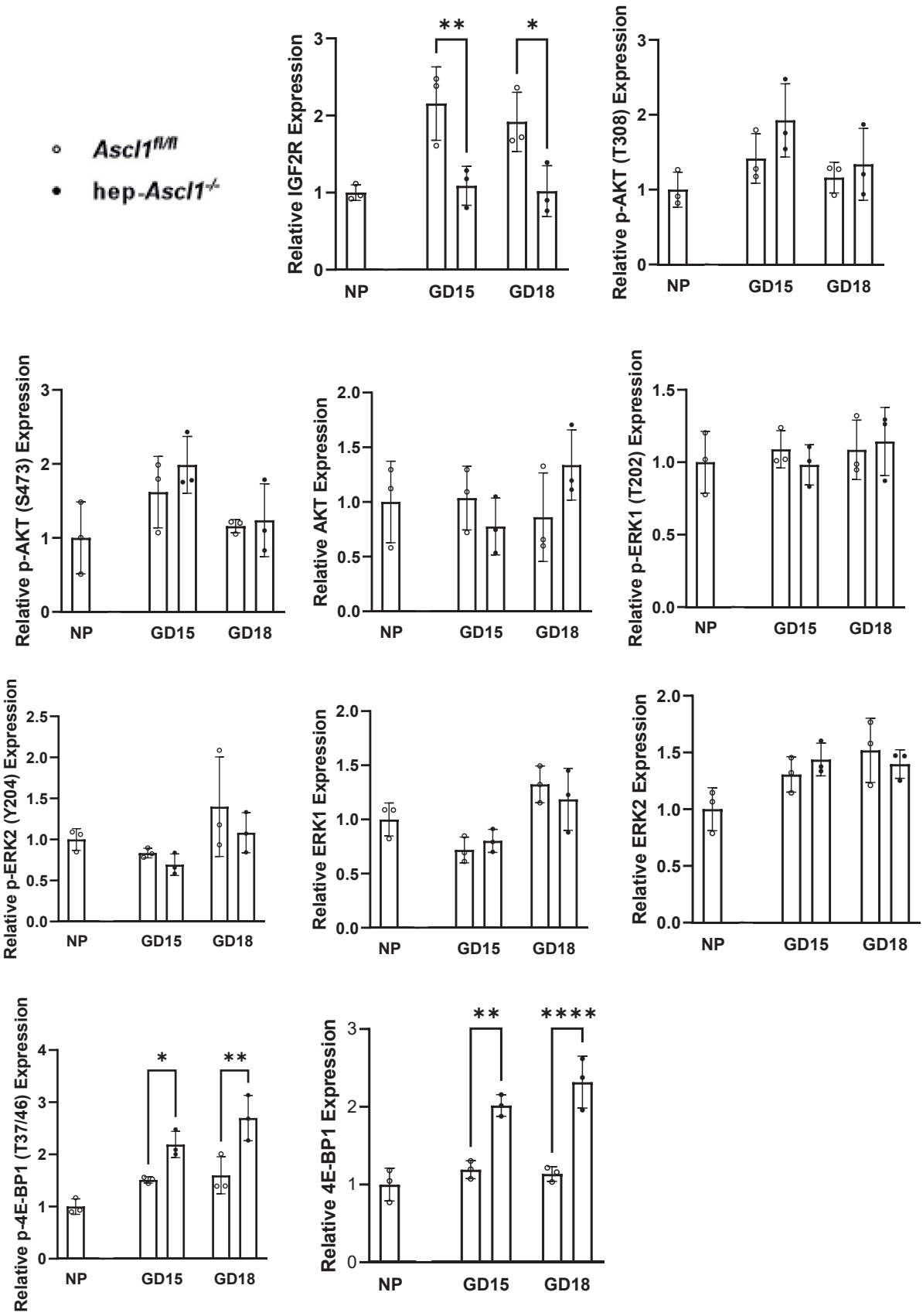

Figure 12. Quantification of the relative intensity of Western blot signals from Figure 11*B*. Signal intensity was normalized with glyceraldehyde 3-phosphate dehydrogenase (GAPDH). Data are presented as the mean fold changes relative to the nonpregnant (NP) state ± SD (n = 3). *$P < .05$, **$P < .01$, and ****$P < .0001$.

Table 1. Primers for Promoter-Specific Igf2 Transcripts

Primer name	Sequence 5' -> 3'
Igf2-all_F	CGGCTTCTACTTCAGCAGGC
Igf2-all_R	GTATCTGGGGAAGTCGTCCG
Igf2-P0_F	TTTATCCACCGTCCGGGAAC
Igf2-P0_R	GCAGTCGTCGTAGTCGTTCT
Igf2-P1_F	CGGCAGCACAGATTTTGGAA
Igf2-P1_R	CACCAACATCGACTTCCCCA
Igf2-P2_F	CCCCAGCCCTAAGATACCCTAA
Igf2-P2_R	AGCACCAACATCGACTTCCC
Igf2-P3_F	CGGCCTCCTTACCCAACTTC
Igf2-P3_R	GGGGTGGCACAGTATGTCTC
18S_F	CTCAACACGGGAAACCTCAC
18S_R	CGCTCCACCAACTAAGAACG

F, forward; R, reverse.

Tissue Collection and Histology

Mice were killed at various time points. Maternal liver, pancreas, spleen, and kidney organs, and placentas and fetuses were collected and weighed. Part of each tissue was fixed in 10% neutral buffered formalin, embedded in paraffin, and sectioned at 5 μm for H&E staining and histologic analysis. Meanwhile, part of each tissue was embedded in optimal cutting temperature compound (23-730-571; Fisher Scientific, Hampton, NH) on heptane cooled in dry ice and stored at -80°C until processing. The remaining tissues were snap-frozen in liquid nitrogen and stored at -80°C for protein and RNA extraction.

Immunohistochemistry

Formalin-fixed, paraffin-embedded maternal liver sections were subjected to standard immunohistochemistry. Primary antibodies against β-catenin (610153, 1:100; BD Transduction, **San Jose, CA**), IGF2 (AF792, 1:1000; R&D Systems, Minneapolis, MN), and Ki67 (RM-9106-S1, 1:100; Thermo Fisher Scientific, Waltham, MA) were used for immunostaining. The slide images were acquired by the Leica DM2000 microscope using the Leica Application Suite program. β-catenin–positive or Ki67-positive hepatocytes in 5 random fields of view at 400× magnification were counted using ImageJ software (National Institutes of Health, Bethesda, MD).[60] Periodic acid–Schiff staining was performed on formalin-fixed, paraffin-embedded placental sections in 0.5% periodic acid solution (sc-215695; Santa Cruz, Dallas, TX) and counterstained in hematoxylin (3801575; Leica, Buffalo Grove, IL).

Western Blot

Liver and placental homogenates (10–30 μg) were separated by polyacrylamide gel electrophoresis under reducing conditions and transferred to polyvinylidene difluoride membranes. The following antibodies were used: phospho-AKT (T308, ab76297, 1:5000; Abcam, Cambridge MA), phospho-AKT (S473, 2118-1, 1:2000; Epitomics, Burlingame, CA), ASCL1 (BAF2567, 1:500; R&D Systems), ERK1/2 (9102, 1:2000; Cell Signaling, Danvers, MA), phospho-ERK1/2 (T202/Y204, 4377, 1:2000; Cell Signaling), glyceraldehyde 3-phosphate dehydrogenase (5174, 1:2000; Cell Signaling), IGF2 (A2086, 1:1000; ABclonal, Woburn, MA), Lamin B1 (9087, 1:1000; Cell Signaling), IGF2R (14364, 1:2000; Cell Signaling), p-4E-BP1 (T37/46) (2855, 1:2000; Cell Signaling), 4E-BP1 (9644, 1:2000; Cell Signaling), and PL-II (1:2000; a gift from Dr Soares at the University of Kansas Medical Center). Immune complexes were detected by SuperSignal West Pico PLUS Chemiluminescent Substrate (34577; Thermo Fisher Scientific). Signals were detected using ImageQuant LAS 4000 Mini (General Electric Life Sciences, Marlborough, MA) and quantified using ImageJ software.[60]

ISH

ISH was performed using the RNAscope 2.5 HD Assay (322310 and 322360; Advanced Cell Diagnostics, Newark, CA) and appropriate probes and as per the manufacturer's directions. The following probes were used: Ascl1 (476321; Advanced Cell Diagnostics), Igf2 (437671; Advanced Cell Diagnostics), PL-I (405521; Advanced Cell Diagnostics), and PL-II (423681; Advanced Cell Diagnostics). A positive control probe Ppib (310043; Advanced Cell Diagnostics) and a negative control probe DapB (313911; Advanced Cell Diagnostics) were used to determine the efficacy of the protocol. These probes were applied to formalin-fixed, paraffin-embedded sections of mouse livers and placentas. The slide images were acquired by the Leica DM2000 microscope using the Leica Application Suite program. After approval from the institutional review boards, the laboratory information systems of our institute were searched. A set of paraffin blocks archived in the Department of Pathology of Indiana University School of Medicine were selected. They represented liver tissues from pregnant patients and patients with hepatocellular carcinoma or hepatocellular adenoma. These paraffin blocks were sectioned for ISH with a human Ascl1 probe (459721; Advanced Cell Diagnostics).

qRT-PCR

Total RNA was isolated from snap-frozen liver tissue using TRIzol reagent (15596018; Invitrogen, Waltham, MA) as per the manufacturer's directions. Complementary DNA (cDNA) was synthesized from 1 μg total RNA using the Verso cDNA kit (AB1453B; Thermo Fisher Scientific) and diluted 4 times with water. qRT-PCR was performed using the diluted cDNA with either TaqMan Gene Expression Master Mix (4369016; Applied Biosystems, Carlsbad, CA) or PowerUp SYBR Green Master Mix (A25742; Applied Biosystems) with specific gene probes.[61] qRT-PCR was performed using the 7300 Real-Time PCR System (Applied Biosystems) and analyzed by the 7300 System SDS RQ Study Software (Applied Biosystems). qRT-PCR conditions for probes (Ascl1: Mm03058063_m1, 4453320; Igf2: Mm00439564_m1, 4331182; Hamp2: Mm03928990_g1, 4453320; 18S: Mm03928990_g1, 4453320; Applied

Biosystems) using TaqMan Gene Expression Master Mix were uracil N-glycosylase incubation (50°C for 2 minutes), polymerase activation (95°C for 10 minutes), and 40 cycles of PCR (95°C for 15 seconds, 60°C for 1 minute). qRT-PCR conditions using PowerUp SYBR Green Master Mix were uracil-DNA glycosylase activation (50°C for 2 minutes), polymerase activation (95°C for 2 minutes), 40 cycles of PCR (95°C for 15 seconds, 60°C for 15 seconds, 72°C for 1 minute), and dissociation curve (95°C for 15 seconds, 60°C for 30 seconds, 95°C for 15 seconds). Primers for detecting promoter-specific Igf2 transcripts are listed in Table 1. Relative gene expression was calculated by the comparative C_T method (ΔΔCt) and normalized to 18S ribosomal RNA transcript levels.

RNA-seq

Total RNA was isolated from snap-frozen liver tissue using the RNeasy Plus Mini Kit (74134; Qiagen, Germantown, MD) as per the manufacturer's directions. RNA sequencing was performed and analyzed by the Center for Medical Genomics Core (Indiana University School of Medicine). In brief, total RNA concentration and quality were assessed using the Agilent 2100 Bioanalyzer (Santa Clara, CA). Single-indexed, strand-specific cDNA library from total RNA samples (500 ng input with RIN $\geq$5) was prepared using the TruSeq Stranded mRNA Library Prep Kit (Illumina) as per the manufacturer's directions. The quality and size distribution of the libraries were assessed using the Qubit (New York, NY) and Agilent 2100 Bioanalyzer. Libraries (200 pmol/L) were clustered and amplified on cBot using the HiSeq 3000/4000 PE Cluster Kit and sequenced (2×75 bp paired-end reads) on a HiSeq4000 (Illumina, San Diego, CA) using the HiSeq 3000/4000 PE SBS Kit. A Phred quality score (Q score) was used to measure the quality of sequencing. The quality of the sequencing data was assessed using FastQC (Babraham Bioinformatics, Cambridge, UK). All sequenced libraries were mapped to the mouse genome (University of California, Santa Cruz [UCSC] mm10) using the STAR RNA-seq aligner (Illumina), reads distribution across the genome was assessed using bamutils (from ngsutils), and uniquely mapped sequencing reads were assigned to mm10 refGene genes using featureCounts (from subread). Genes with CPM less than 0.5 in more than 5 of the samples were removed. The data were normalized using the Trimmed Mean of M-values (TMM) method. Differential expression analysis was performed using edgeR (Bioconductor) and Ingenuity Pathway Analysis with ±2-fold change and $P < .05$. The false-discovery rate was computed from P values using the Benjamini–Hochberg procedure.

Serum Biochemistry

Blood from nonpregnant and pregnant mice (GD15 and GD18) was collected and left to clot at room temperature. After 2 centrifugations at 3000 rpm, serum was collected and analyzed by Eli Lilly and Company (Indianapolis, IN). Serum insulin levels were measured by the Translation Core at the Indiana University School of Medicine Center for Diabetes and Metabolic Diseases. Serum IGF2 levels were quantified using a one-sixth dilution with the Mouse IGF2 ELISA Kit (EK0381; Boster Biological Technology, Pleasanton, CA) as per the manufacturer's directions and read with the SpectraMax M2e spectrophotometer (Molecular Devices, San Jose, CA) using the SoftMax Pro 6 program (Molecular Devices).

Microbiome 16S Sequencing

Total microbial DNA was isolated from the snap-frozen cecal sample using the PureLink Microbiome DNA Purification Kit (A29789; Invitrogen) as per the manufacturer's directions. Microbiome 16S sequencing was performed and analyzed by the Zymo Research Corporation (Irvine, CA). In brief, bacterial 16S ribosomal RNA gene-targeted sequencing was performed using the Quick-16S NGS Library Preparation Kit (Zymo Research). The bacterial 16S primers, custom-designed by Zymo Research, amplified the V3–V4 region of the 16S ribosomal RNA gene. The sequencing library was prepared using PCR reactions in real-time PCR machines to control cycles and therefore prevent PCR chimera formation. The final PCR products were quantified with qPCR fluorescence readings and pooled together based on equal molarity. The final pooled library was cleaned up with Select-a-Size DNA Clean and Concentrator (Zymo Research), and then quantified with TapeStation (Agilent) and Qubit (Thermo Fisher Scientific). The final library was sequenced on an Illumina MiSeq with a v3 reagent kit (600 cycles). The sequencing was performed with more than 10% PhiX (Illumina) spike-in. Amplicon sequences were inferred from raw reads using the Dada2 (Bioconductor) pipeline. Chimeric sequences also were removed with the Dada2 pipeline. Taxonomy assignment, composition bar charts, α-diversity, and β-diversity analyses were performed with Qiime v.1.9.1 (University of Colorado Boulder, Boulder, CO). Taxa that had an abundance that was significantly different among groups was identified by linear discriminant analysis effect size (LEfSe) with default settings if applicable. Differential expression analysis was assessed using Ingenuity Pathway Analysis with ±2-fold change and $P < .05$.

β-Cell Mass

Pancreatic tissues were fixed in 4% paraformaldehyde (818715; Sigma Aldrich, St. Louis, MO), embedded in paraffin, and sectioned at 7 μm for collecting 5 sections at 50-μm apart per pancreatic sample. Pancreatic sections immunostained for insulin (sc-9168, 1:100; Santa Cruz) were used to quantify insulin-positive β-cell mass. β-cell mass was determined by the ratio of the insulin-positive stained area to the tissue area multiplied by the pancreas weight.

Statistical Analysis

Data are shown as means ± SD or means ± SEM. Statistical analyses were performed using 1-way analysis of variance with Sidak multiple comparisons or a 2-sided unpaired Student t test with the means ± 95% CIs. Significant differences were defined when $P < .05$.

All authors had access to the study data and reviewed and approved the final manuscript.

References

1. Dai G, Bustamante JJ, Zou Y, Myronovych A, Bao Q, Kumar S, Soares MJ. Maternal hepatic growth response to pregnancy in the mouse. Exp Biol Med (Maywood) 2011;236:1322–1332.
2. Huang C, Snider F, Cross JC. Prolactin receptor is required for normal glucose homeostasis and modulation of beta-cell mass during pregnancy. Endocrinology 2009;150:1618–1626.
3. van der Giessen J, Binyamin D, Belogolovski A, Frishman S, Tenenbaum-Gavish K, Hadar E, Louzoun Y, Peppelenbosch MP, van der Woude CJ, Koren O, Fuhler GM. Modulation of cytokine patterns and microbiome during pregnancy in IBD. Gut 2020;69:473–486.
4. Maymon R, Strauss S, Vaknin Z, Weinraub Z, Herman A, Gayer G. Normal sonographic values of maternal spleen size throughout pregnancy. Ultrasound Med Biol 2006; 32:1827–1831.
5. Bustamante JJ, Dai G, Soares MJ. Pregnancy and lactation modulate maternal splenic growth and development of the erythroid lineage in the rat and mouse. Reprod Fertil Dev 2008;20:303–310.
6. Beydoun SN. Morphologic changes in the renal tract in pregnancy. Clin Obstet Gynecol 1985;28:249–256.
7. Roy C, Saussine C, Jahn C, Le Bras Y, Steichen G, Delepaul B, Campos M, Chambron J, Jacqmin D. Fast imaging MR assessment of ureterohydronephrosis during pregnancy. Magn Reson Imaging 1995;13:767–772.
8. Dunlop W. Serial changes in renal haemodynamics during normal human pregnancy. Br J Obstet Gynaecol 1981;88:1–9.
9. Ryan JM, Heneghan MA. Pregnancy and the liver. Clin Liver Dis 2014;4:51–54.
10. Frederiksen MC. Physiologic changes in pregnancy and their effect on drug disposition. Semin Perinatol 2001; 25:120–123.
11. Guillemot F, Lo LC, Johnson JE, Auerbach A, Anderson DJ, Joyner AL. Mammalian achaete-scute homolog 1 is required for the early development of olfactory and autonomic neurons. Cell 1993;75:463–476.
12. Casarosa S, Fode C, Guillemot F. Mash1 regulates neurogenesis in the ventral telencephalon. Development 1999;126:525–534.
13. Horton S, Meredith A, Richardson JA, Johnson JE. Correct coordination of neuronal differentiation events in ventral forebrain requires the bHLH factor MASH1. Mol Cell Neurosci 1999;14:355–369.
14. Bustamante JJ, Copple BL, Soares MJ, Dai G. Gene profiling of maternal hepatic adaptations to pregnancy. Liver Int 2010;30:406–415.
15. Bertrand N, Castro DS, Guillemot F. Proneural genes and the specification of neural cell types. Nat Rev Neurosci 2002;3:517–530.
16. Imayoshi I, Isomura A, Harima Y, Kawaguchi K, Kori H, Miyachi H, Fujiwara T, Ishidate F, Kageyama R. Oscillatory control of factors determining multipotency and fate in mouse neural progenitors. Science 2013;342:1203–1208.
17. Meredith A, Johnson JE. Negative autoregulation of Mash1 expression in CNS development. Dev Biol 2000; 222:336–346.
18. Altree-Tacha D, Tyrrell J, Li F. mASH1 is highly specific for neuroendocrine carcinomas: an immunohistochemical evaluation on normal and various neoplastic tissues. Arch Pathol Lab Med 2017;141:288–292.
19. Yanger K, Zong Y, Maggs LR, Shapira SN, Maddipati R, Aiello NM, Thung SN, Wells RG, Greenbaum LE, Stanger BZ. Robust cellular reprogramming occurs spontaneously during liver regeneration. Genes Dev 2013;27:719–724.
20. Ho KJ, Bass CE, Kroemer AH, Ma C, Terwilliger E, Karp SJ. Optimized adeno-associated virus 8 produces hepatocyte-specific Cre-mediated recombination without toxicity or affecting liver regeneration. Am J Physiol Gastrointest Liver Physiol 2008;295:G412–G419.
21. Wang L, Wang H, Bell P, McCarter RJ, He J, Calcedo R, Vandenberghe LH, Morizono H, Batshaw ML, Wilson JM. Systematic evaluation of AAV vectors for liver directed gene transfer in murine models. Mol Ther 2010; 18:118–125.
22. Koren O, Goodrich JK, Cullender TC, Spor A, Laitinen K, Backhed HK, Gonzalez A, Werner JJ, Angenent LT, Knight R, Backhed F, Isolauri E, Salminen S, Ley RE. Host remodeling of the gut microbiome and metabolic changes during pregnancy. Cell 2012;150:470–480.
23. Zhu C, Song K, Shen Z, Quan Y, Tan B, Luo W, Wu S, Tang K, Yang Z, Wang X. Roseburia intestinalis inhibits interleukin-17 excretion and promotes regulatory T cells differentiation in colitis. Mol Med Rep 2018; 17:7567–7574.
24. López-Cortés A, Fardeau M-L, Fauque G, Joulian C, Ollivier B. Reclassification of the sulfate- and nitrate-reducing bacterium Desulfovibrio vulgaris subsp. oxamicus as Desulfovibrio oxamicus sp. nov., comb. nov. Int J Syst Evol Microbiol 2006;56:1495–1499.
25. Liu ZM, Chen J, Lv YP, Hu ZH, Dai QM, Fan XL. Molecular characterization of a hepcidin homologue in starry flounder (Platichthys stellatus) and its synergistic interaction with antibiotics. Fish Shellfish Immunol 2018; 83:45–51.
26. Gui L, Zhang P, Zhang Q, Zhang J. Two hepcidins from spotted scat (Scatophagus argus) possess antibacterial and antiviral functions in vitro. Fish Shellfish Immunol 2016;50:191–199.
27. Simmons DG, Rawn S, Davies A, Hughes M, Cross JC. Spatial and temporal expression of the 23 murine prolactin/placental lactogen-related genes is not associated with their position in the locus. BMC Genomics 2008; 9:352.
28. Bergman D, Halje M, Nordin M, Engstrom W. Insulin-like growth factor 2 in development and disease: a mini-review. Gerontology 2013;59:240–249.
29. Constancia M, Hemberger M, Hughes J, Dean W, Ferguson-Smith A, Fundele R, Stewart F, Kelsey G,

Fowden A, Sibley C, Reik W. Placental-specific IGF-II is a major modulator of placental and fetal growth. Nature 2002;417:945–948.

30. Sferruzzi-Perri AN, Sandovici I, Constancia M, Fowden AL. Placental phenotype and the insulin-like growth factors: resource allocation to fetal growth. J Physiol 2017;595:5057–5093.
31. Soares MJ. The prolactin and growth hormone families: pregnancy-specific hormones/cytokines at the maternal-fetal interface. Reprod Biol Endocrinol 2004;2:51.
32. Campbell WJ, Larsen D, Deb S, Kwok SC, Soares MJ. Expression of alkaline phosphatase in differentiated rat labyrinthine trophoblast tissue. Placenta 1991; 12:227–237.
33. Kent LN, Ohboshi S, Soares MJ. Akt1 and insulin-like growth factor 2 (Igf2) regulate placentation and fetal/postnatal development. Int J Dev Biol 2012;56:255–261.
34. Kuida K, Boucher DM. Functions of MAP kinases: insights from gene-targeting studies. J Biochem 2004; 135:653–656.
35. Rotwein P, Hall LJ. Evolution of insulin-like growth factor ii: characterization of the mouse IGF-II gene and identification of two pseudo-exons. DNA Cell Biol 1990; 9:725–735.
36. Tabata H, Kobayashi M, Ikeda JH, Nakao N, Saito TR, Tanaka M. Characterization of multiple first exons in murine prolactin receptor gene and the effect of prolactin on their expression in the choroid plexus. J Mol Endocrinol 2012;48:169–176.
37. Lu L, Li Y, Kim SM, Bossuyt W, Liu P, Qiu Q, Wang Y, Halder G, Finegold MJ, Lee J-S, Johnson RL. Hippo signaling is a potent in vivo growth and tumor suppressor pathway in the mammalian liver. Proc Natl Acad Sci U S A 2010;107:1437–1442.
38. Brouwer-Visser J, Huang GS. IGF2 signaling and regulation in cancer. Cytokine Growth Factor Rev 2015; 26:371–377.
39. Liu J, Hu X, Chen J, Li X, Wang L, Wang B, Peng W, Yang C, Li Z, Chen Y, Wang YJ, Li C, Li X, Yan F, Wang Y, Shang C, Wang X, Chen T, Huang P. Pericentral hepatocytes produce insulin-like growth factor-2 to promote liver regeneration during selected injuries in mice. Hepatology 2017;66:2002–2015.
40. Hassan AB. Keys to the hidden treasures of the mannose 6-phosphate/insulin-like growth factor 2 receptor. Am J Pathol 2003;162:3–6.
41. Qin X, Jiang B, Zhang Y. 4E-BP1, a multifactor regulated multifunctional protein. Cell Cycle 2016;15:781–786.
42. Pattyn A, Simplicio N, van Doorninck JH, Goridis C, Guillemot F, Brunet JF. Ascl1/Mash1 is required for the development of central serotonergic neurons. Nat Neurosci 2004;7:589–595.
43. Peltopuro P, Kala K, Partanen J. Distinct requirements for Ascl1 in subpopulations of midbrain GABAergic neurons. Dev Biol 2010;343:63–70.
44. Chanda S, Ang CE, Davila J, Pak C, Mall M, Lee QY, Ahlenius H, Jung SW, Sudhof TC, Wernig M. Generation of induced neuronal cells by the single reprogramming factor ASCL1. Stem Cell Rep 2014;3:282–296.
45. Li J, Neumann I, Volkmer I, Staege MS. Down-regulation of achaete-scute complex homolog 1 (ASCL1) in neuroblastoma cells induces up-regulation of insulin-like growth factor 2 (IGF2). Mol Biol Rep 2011;38:1515–1521.
46. Konstantinov SR, van der Woude CJ, Peppelenbosch MP. Do pregnancy-related changes in the microbiome stimulate innate immunity? Trends Mol Med 2013;19:454–459.
47. Mulligan CM, Friedman JE. Maternal modifiers of the infant gut microbiota: metabolic consequences. J Endocrinol 2017;235:R1–R12.
48. Fox JG, Dewhirst FE, Tully JG, Paster BJ, Yan L, Taylor NS, Collins MJ Jr, Gorelick PL, Ward JM. Helicobacter hepaticus sp. nov., a microaerophilic bacterium isolated from livers and intestinal mucosal scrapings from mice. J Clin Microbiol 1994;32:1238–1245.
49. Yang JY, Lee YS, Kim Y, Lee SH, Ryu S, Fukuda S, Hase K, Yang CS, Lim HS, Kim MS, Kim HM, Ahn SH, Kwon BE, Ko HJ, Kweon MN. Gut commensal Bacteroides acidifaciens prevents obesity and improves insulin sensitivity in mice. Mucosal Immunol 2017; 10:104–116.
50. Kanauchi O, Fujiyama Y, Mitsuyama K, Araki Y, Ishii T, Nakamura T, Hitomi Y, Agata K, Saiki T, Andoh A, Toyonaga A, Bamba T. Increased growth of Bifidobacterium and Eubacterium by germinated barley foodstuff, accompanied by enhanced butyrate production in healthy volunteers. Int J Mol Med 1999; 3:175–179.
51. Bereswill S, Ekmekciu I, Escher U, Fiebiger U, Stingl K, Heimesaat MM. Lactobacillus johnsonii ameliorates intestinal, extra-intestinal and systemic pro-inflammatory immune responses following murine Campylobacter jejuni infection. Sci Rep 2017;7:2138.
52. Lu S, Seravalli J, Harrison-Findik D. Inductively coupled mass spectrometry analysis of biometals in conditional Hamp1 and Hamp1 and Hamp2 transgenic mouse models. Transgenic Res 2015;24:765–773.
53. Pigeon C, Ilyin G, Courselaud B, Leroyer P, Turlin B, Brissot P, Loreal O. A new mouse liver-specific gene, encoding a protein homologous to human antimicrobial peptide hepcidin, is overexpressed during iron overload. J Biol Chem 2001;276:7811–7819.
54. Catalano PM, Shankar K. Obesity and pregnancy: mechanisms of short term and long term adverse consequences for mother and child. BMJ 2017;356:j1.
55. Dunlop AL, Mulle JG, Ferranti EP, Edwards S, Dunn AB, Corwin EJ. Maternal microbiome and pregnancy outcomes that impact infant health: a review. Adv Neonatal Care 2015;15:377–385.
56. Chen X, Zhao D, Mao X, Xia Y, Baker PN, Zhang H. Maternal dietary patterns and pregnancy outcome. Nutrients 2016;8:351.
57. Andersen J, Urbán N, Achimastou A, Ito A, Simic M, Ullom K, Martynoga B, Lebel M, Göritz C, Frisén J, Nakafuku M, Guillemot F. A transcriptional mechanism integrating inputs from extracellular signals to activate hippocampal stem cells. Neuron 2014;83:1085–1097.
58. Truett GE, Heeger P, Mynatt RL, Truett AA, Walker JA, Warman ML. Preparation of PCR-quality mouse genomic

DNA with hot sodium hydroxide and tris (HotSHOT). Biotechniques 2000;29(52):54.

59. Pacary E, Heng J, Azzarelli R, Riou P, Castro D, Lebel-Potter M, Parras C, Bell Donald M, Ridley Anne J, Parsons M, Guillemot F. Proneural transcription factors regulate different steps of cortical neuron migration through rnd-mediated inhibition of RhoA signaling. Neuron 2011;69:1069–1084.
60. Schneider CA, Rasband WS, Eliceiri KW. NIH Image to ImageJ: 25 years of image analysis. Nat Methods 2012; 9:671–675.
61. Yang P, Wang Y, Hoang D, Tinkham M, Patel A, Sun M-A, Wolf G, Baker M, Chien H-C, Lai K-YN, Cheng X, Shen C-KJ, Macfarlan TS. A placental growth factor is silenced in mouse embryos by the zinc finger protein ZFP568. Science 2017;356:757–759.

Received May 1, 2021. Accepted August 10, 2021.

Correspondence
Address correspondence to: Huaizhou Jiang, MD, PhD, or Guoli Dai, DVM, PhD, Department of Biology, School of Science, Indiana University–Purdue University Indianapolis, 723 West Michigan Street, SL306, Indianapolis, Indiana 46202. e-mail: huajiang@iu.edu; gdai@iupui.edu; fax: (317) 274-2846.

Acknowledgment
The authors thank Dr Michael J. Soares at the University of Kansas Medical Center and Dr Jane Johnson at the University of Texas Southwestern Medical Center for critically reading the manuscript and their valuable comments and suggestions.

CRediT Authorship Contributions

Joonyong Lee (Conceptualization: Lead; Data curation: Lead; Formal analysis: Lead; Investigation: Lead; Methodology: Lead; Writing – original draft: Lead)

Veronica Garcia (Conceptualization: Supporting; Data curation: Supporting; Formal analysis: Lead; Investigation: Supporting; Methodology: Lead)

Shashank Nambiar (Data curation: Supporting)

Huaizhou Jiang (Conceptualization: Lead; Data curation: Supporting; Investigation: Supporting; Writing – original draft: Lead)

Guoli Dai, PhD (Conceptualization: Lead; Funding acquisition: Lead; Investigation: Lead; Methodology: Lead; Resources: Lead; Supervision: Lead; Writing – original draft: Lead)

Conflicts of interest
The authors disclose no conflicts.

Funding
This work was supported by a grant from the National Institute of Diabetes and Digestive and Kidney Diseases (1R01DK117076) and by a pilot grant from the Center for Diabetes and Metabolic Diseases of Indiana University School of Medicine.